Hepatocyte Autotaxin expression promotes liver fibrosis and cancer

Eleanna Kaffe[1], Aggeliki Katsifa[1], Nikos Xylourgidis[1], Ioanna Ninou[1], Markella Zannikou[1], Vaggelis Harokopos[1], Pelagia Foka[2], Alexios Dimitriadis[2], Kostas Evangelou[3], Anargyros N. Moulas[4], Urania Georgopoulou[2], Vassilis G. Gorgoulis[3,5,6], George N. Dalekos[7] and Vassilis Aidinis[1]

From the [1]Division of Immunology, Biomedical Sciences Research Center Alexander Fleming, Athens, Greece; [2]Laboratory of Molecular Virology, Hellenic Pasteur Institute, Athens, Greece; [3]Department of Histology and Embryology, School of Medicine, University of Athens, Athens, Greece; [4]Laboratory of Biochemistry, Technological Educational Institute of Thessaly, Larissa, Greece; [5]Biomedical Research Foundation, Academy of Athens, Athens, Greece; [6]Institute for Cancer Sciences, University of Manchester, Manchester Academic Health Science Centre, Manchester, UK; [7]Department of Medicine and Research Laboratory of Internal Medicine, Medical School, University of Thessaly, Larissa, Greece.

Keywords: lipidomics, lysophospholipids, hepatic stellate cells

Correspondence: Vassilis Aidinis, Division of Immunology, Biomedical Sciences Research Center Alexander Fleming, 34 Fleming Street, 16672 Athens, Greece. Phone: +302109654382; E-mail: V.Aidinis@Fleming.gr.

Abbreviations: ATX, Autotaxin; CCl_4, carbon tetrachloride; ConA, concanavalin A; HA, hyaluronic acid; Heps, hepatocytes; HSCs, hepatic stellate cells; IP, intraperitoneally; LPA, lysophosphatidic acid; LPAR, LPA receptor; LPC, lysophoshatidylcholine; Ppap2, phospholipid phosphatases; PLA2, phospholipase A2.

This article has been accepted for publication and undergone full peer review but has not been through the copyediting, typesetting, pagination and proofreading process which may lead to differences between this version and the Version of Record. Please cite this article as doi: 10.1002/hep.28973

Abstract

Autotaxin (ATX) is a secreted lysophospholipase D catalyzing the production of lysophosphatidic acid (LPA), a pleiotropic growth factor-like lysophospholipid. Increased ATX expression has been detected in various chronic inflammatory disorders and different types of cancer; however little is known about its role and mode of action in liver fibrosis and cancer. Here, increased ATX expression was detected in chronic liver diseases (CLDs) patients of different etiologies, associated with shorter overall survival. In mice, different hepatotoxic stimuli linked with the development of different forms of CLDs were shown to stimulate hepatocyte ATX expression, leading to increased LPA levels, the activation of hepatic stellate cells (HSCs) and the amplification of pro-fibrotic signals. Hepatocyte-specific, conditional genetic deletion and/or transgenic overexpression of ATX established a liver pro-fibrotic role for ATX/LPA, while pharmacologic ATX inhibition studies suggested ATX as a possible therapeutic target in CLDs. In addition, hepatocyte ATX ablation and the consequent deregulation of lipid homeostasis was also shown to attenuate HCC development, thus implicating ATX/LPA in the causative link of cirrhosis and HCC. *Conclusion*: ATX is a novel player in the pathogenesis of liver fibrosis and cancer and a promising therapeutic target.

Introduction

Several chronic liver disorders (CLDs), including chronic viral hepatitis (CVH), alcoholic liver disease (ALD) and non-alcoholic fatty liver disease/non-alcoholic steatohepatitis (NAFLD/NASH), cause hepatocellular injury and necrosis, triggering in turn inflammation and a wound-healing response characterized by the accumulation of ECM. If the insult is acute or self-limited, wound healing responses quickly restore normal tissue homeostasis and liver architecture. However, if the insult persists, the ensuing chronic inflammation and ECM accumulation overrides the ability of liver to regenerate, leading to fibrosis and ultimately to cirrhosis, a liver disorder with dismal prognosis and the major risk factor for the development of HCC.[1]

ATX is a secreted lysophospholipase D catalyzing the hydrolysis of lysophosphatidylcholine (LPC) to LPA, a pleiotropic growth factor like phospholipid.[2] LPA has numerous effects in almost all cell types through its G-protein coupled receptors (GPCR; LPAR1-6) which exhibit overlapping specificities and widespread distribution.[3] Upregulated ATX expression has been detected in various chronic inflammatory disorders and different types of cancer.[4,5] ATX was shown to play a decisive role in the development of pulmonary fibrosis;[6] however little is known about its role and mode of action in other fibroproliferative diseases.

Expanding and complementing previous studies,[7] we have shown increased serum ATX levels in CLDs of different etiologies, correlating with decreased survival, as well as increased liver ATX mRNA expression in both CLD and HCC patients. Accordingly, increased hepatocyte ATX and liver LPA expression was shown in animal models of experimental toxic hepatitis and HCC. Genetic and pharmacologic interventions *in vivo*, coupled with *ex vivo* studies indicated that ATX disturbs lipid homeostasis and promotes the development both fibrosis and cancer.

Materials and Methods

Human Subjects. Clinical and personal characteristics of patients are presented at Supporting Table S2. Clinical investigations have been conducted according to Declaration of Helsinki principles. All patients and controls consented for anonymous research usage of their samples, as approved by the Ethical Committee of the University of Thessaly Medical School.

Animal Experimentation. All experimental mice, were bred and maintained in a C57Bl6/J genetic background (>10 generations) under SPF conditions at 20–22^{o}C, 55±5% humidity, and a 12-h light-dark cycle; water and food (irradiated standard diet Mucedola # 4RF21) were provided *ad libitum*. The generation and genotyping protocols for *Enpp2*$^{n/n}$,[8] Tg*Alb-Cre*,[9] R26R[10] and Tg*a1t1-hEnpp2*[11] mice have been described previously. All randomly-assigned experimental controls were littermate sex- and age-matched mice. All reported experimentation in mice for this project, in line with the ARRIVE guidelines, was approved by the Institutional Animal Ethical Committee (#377) and the Veterinary service and Fishery Department of the local governmental prefecture (#5366).

Acute and chronic intoxication with diethylnitrosamine (DEN) and/or carbon tetrachloride (CCl_4), liver histology, hepatic cell isolation and HCV infection, HPLC-ESI/MS/MS, ATX activity assay (TOOS), ELISA and western blot, and RNA Extraction and Real-time RT-PCR, are described in Supporting Information.

Statistical Analysis is indicated accordingly at the individual figure legends**.**

Results

Increased ATX expression in CLD patients of different aetiologies. To interrogate human patients liver mRNA expression of ATX, as well as of LPA receptors (*LPAR1-6*) and phospholipid phosphatases (*PPAP2A-C/LPP1-3*), we performed data mining in all CLD patient microarray datasets publically available at NCBI/GEO (Table S1A). Statistically significant increased ATX mRNA expression was found in the majority of data sets/patient cohorts; the same is true for *LPAR6*, previously suggested to support the tumorigenicity of HCC.[12] Similarly, increased ATX mRNA levels were also detected in HCC data sets (Table S1B), accompanied by decreased expression of *PPA2PB* suggested to mediate LPA turnover.[13]

Increased ATX sera levels were identified in patients with CVH (including HCV and hepatitis B virus - HBV), as well as in ALD and NASH patients (Fig. 1A; Table S2), suggesting ATX as a biomarker in all CLDs regardless of the initiating insult. Noteworthy, the CVH patient group, exhibiting a large number of values close to the normal range, included 18 samples from patients with inactive disease as a result of the appropriate antiviral treatment. Interestingly, ATX levels in responding patients were significantly lower (155 (43-467) ng/ml, p=0.04) than 17 treatment-naive CVH patients with an active disease (as defined by biochemical activity and/or viral replication)(285 (109-3500) ng/ml).

Significant, albeit weak, associations of serum ATX levels were also discovered with a number of surrogate disease parameters (Table S3), including AST/ALT and bilirubin, indicative of hepatic damage and loss of function respectively. Importantly, low serum ATX levels were significantly associated with longer overall survival in a 10 year follow up period (Fig. 1B), further suggesting ATX as a prognostic indicator of disease severity.

Increased, well-timed liver ATX expression in experimental toxic hepatitis. Chronic exposure to CCl_4 resulted, as expected, to focal, confluent and portal necrosis, followed by portal inflammatory infiltration (Fig. S1A,B) of different cell types (Fig. S1C-J). Apoptosis ($TUNEL^+$ cells) was profound at 4w post CCl_4 administration (Fig. S1K,L), accompanied by a strong regenerative response and Heps proliferation ($PCNA^+$ cells; Fig. S1M,N), as well as increased glycogen and neutral lipids deposition (Fig. S1O-Q). The initial cytotoxic and inflammatory response to CCl_4 chronic administration was followed by a strong fibrotic response (Fig. S1R,S) and gradual collagen deposition (Fig. S2A), leading to hepatic damage at late stages (8-12w; Fig. S2B,C), resulting to aberrant liver clearance functions (Fig. S2D).

Robust liver expression of ATX was detected (Fig. 2A-C) at 4w post CCl_4 administration (as well as after continuous administration of thioacetamide; Fig. S3), following an increased inflammatory gene expression profile (*Tnf*, *Il-1b* and *Il-6*; Fig. S2E). Fibrotic gene expression (*Tgfb*, *aSMA/Acta2*, *Col3a1*) increased gradually throughout disease development (Fig. S2F); however, significant aSMA protein expression was first detected at 4w (Fig. 2C), the peak of ATX expression, accompanied by a major shift in the *Cxcr4*/*Cxcr7* mRNA expression ratio (Fig. S2G), increased *Cyp2S1* mRNA levels (Fig. S2G) and increased plasma levels of retinoic acids (RA; Fig. S2H). Therefore, CCl_4-induced, ATX well-timed liver expression coincided with the expression of several markers of HSC activation, suggesting a role for ATX in the modulation of HSC physiology and the establishment of fibrosis.

Distorted phospholipid homeostasis in experimental toxic hepatitis. To possibly correlate ATX levels with the levels of its enzymatic product LPA, as well as to detect

other possible disturbances in lipid homeostasis, we next performed lipidomic analysis of CCl_4-induced disease progression with HPLC-MS/MS. Clustering of lipid expression levels identified four major groups of lipids with deregulated expression (Fig. 2E).

The first group was composed mainly of LPA species, exhibiting comparatively the highest upregulation in liver tissue, peaking at 4w both in liver tissue and plasma (Fig. 2E, Fig. S4A,B). As in human CLD patients (Table S1A), *Lpar6* exhibited the highest expression in the liver, peaking at 4w (Fig. S2I). Therefore, the increased liver ATX expression upon damage led to local increases of LPA, possibly further sustained by the identified decrease in *Ppap2b* levels (Fig. S2J).

A second group of lipids was composed mainly of LPC species peaking at 4w (Fig. 2E, Fig. S4E,F). Accordingly, most liver abundant phospholipase A2 (*Pla2*) isoforms, largely responsible for liver LPC synthesis, were found upregulated at 2-4w post CCl_4 administration (Fig. S2K). In agreement, expression profiling of all publicly available human CLD datasets as described above, indicated a liver overexpression of PLA2 g4C, g5 and g7 isoforms (Table S1C), suggesting a parallel involvement of the PLA2/LPC axis in the pathogenesis of CLDs and toxin-induced hepatitis.

The third group (Fig. 2E) was composed mainly from TAGs, in agreement with the observed neutral lipid deposition (Fig. S1 O-Q). The last group, a clustering node by itself, was composed mainly of phosphatidyl ethanolamine (PE) and lysoPE (LPE) species that surged in the plasma, most likely as a direct toxic effect of CCl_4 on cell membranes.

Hepatocyte injury or infection stimulates ATX expression. The increased ATX expression in the liver was localized mainly to Heps by double immunolabelling,

which furthermore indicated that aSMA-expressing myofibroblasts are not major producers of ATX (Fig. 3A). Accordingly, fractionated primary Heps were found to produce and secrete the vast majority of ATX (Fig. 3B,C), further confirming the increased Hep ATX expression upon CCl_4 intoxication (Fig. 3D).

ATX expression from Heps (and Kupffer cells) *ex vivo* was stimulated by TNF and LPS (Fig. 3E,F), while elevated liver ATX levels were detected upon Concanavalin A (ConA)-induced, T-cell-dependent and TNF-mediated, inflammatory Heps damage *in vivo* (Fig. S5).[14] Remarkably, ATX expression was also stimulated upon HCV (JFH-1) infection in the permissive Huh7.5 hepatoma cell line or pJFH-1 RNA transfection in Hep2G cells (Fig. S6A,B).

Remarkably, LPC (18:1) was also shown to be a potent stimulus of ATX expression from Heps *ex vivo* (Fig. S6C-D), while promoting their apoptosis (Fig. S6E,F). In agreement, LPC administration (18:1; 60 mg/Kg i.v.) in mice *in vivo* led to an increase of both ATX and apoptosis (Fig. S6G-J), suggesting LPC as a potent ATX inducer in the liver. On the contrary, no major LPA effect in hepatocyte ATX expression was observed (Fig. 3E).[15]

Hepatocyte-specific ATX expression activates HSCs and amplifies the fibrotic response. To examine if Hep-specific ATX expression plays a pathogenic role in the development of liver fibrosis, ATX was genetically deleted from Heps by mating the conditional knockout mouse for ATX ($Enpp2^{n/n}$)[8] with a transgenic mouse line expressing the Cre recombinase under the tight control of the albumin (Alb) promoter (Tg*Alb-Cre*), directing efficient recombination of floxed alleles specifically to Heps (Fig. S7A,B).[9,10] Accordingly, no Hep ATX expression could be detected in $AlbEnpp2^{-/-}$ mice 4w post CCl_4 administration (Fig. 4Aa,B), followed by diminished

liver and plasma LPA levels (Fig. 4C, S7C,D) and a complete reversal of the corresponding lipidomic profiles (Fig. 2E), thus suggesting that CCl_4-induced Heps-specific ATX expression results to local LPA production, that is also reflected in the circulation.

Abrogation of liver ATX/LPA production resulted to diminished necrosis (Fig. 4Ab,D), apoptosis (Fig. S7Ea, Fig. 4D) and proliferation (Fig. S7Eb, Fig. 4D); however, the number of hydropic cells increased in the absence of ATX (Fig. 4Ab,D) suggesting that ATX/LPA might interfere with ionic and/or fluid homeostasis.[16] The overall liver inflammatory histopathological score was not significantly reduced (Fig. 4D), although parenchymal inflammation appeared more diffuse rather than periportal (Fig. 4Ab), inflammatory gene expression was modulated (Fig. S7F) and a reduction in the number of infiltrating $Gr1^+$ cells and activated macrophages was observed (Fig. S7I). Moreover, ATX deletion diminished the deposition of neutral lipids, but had no effect on glycogen deposition (Fig. S7E). More importantly, ATX ablation led to a diminished histopathological fibrotic score (Fig. 4D), consistent with decreased collagen production (Fig. 4E), pro-fibrotic gene expression (Fig. 4F), aSMA expression (Fig. 4Ad), as well as liver damage (Fig. S7G,H).

Conversely, CCl_4 administration to Tg*a1t1-hEnpp2* mice, overexpressing a human ATX transgene in Heps driven by the human α1- antitrypsin inhibitor (a1t1) promoter[11], resulted to increased collagen deposition and fibrosis (Fig. S8). ATX/LPA levels in CCl_4-treated Tg*a1t1-hEnpp2* mice were not significantly higher than CCl_4-treated wt littermates (Fig. S8G-I), as transgenic *a1t1*-driven hATX expression was not CCl_4-induced (Fig. S8J), suggesting that the chronic exposure to LPA rather than its absolute levels exerted the observed pro-fibrotic effect.

In agreement with a chronic role of ATX/LPA pathogenetic effects in liver injury, ATX Heps ablation or overexpression led to minimal changes in the ConA model (Fig. S9 A-D and I-L respectively), suggesting no major effects of ATX in acute, T-cell-dependent and TNF-mediated liver inflammatory responses. Likewise, genetic deletion or overexpression of ATX from Heps had also minor effects in acute (single dose), CCl_4-induced hepatic damage (Fig. S9 E-H and M-P respectively).

Genetic deletion of ATX from hepatocytes had also minor effects in liver regeneration following partial hepatectomy (Fig. S10A,B), suggesting no major effects of ATX/LPA in hepatocyte proliferation, as seen *in vitro* (Fig. S10C,D). LPA stimulated *Tnf*, *Il-6* and *Cxcr4* expression in primary hepatocytes *in vitro* (Fig. S10C), however the relative contribution of LPA-induced hepatocyte responses to the overall liver pro-inflammatory and pro-fibrotic gene expression (Fig. S2E-G) remains unknown.

Despite the minimum involvement of ATX in acute liver damage, deletion or overexpression of ATX, in *AlbEnpp2*$^{-/-}$ or Tg*a1t1-hEnpp2* mice respectively, modulated accordingly *Acta2/aSMA* liver mRNA levels 24h post-acute exposure to CCl_4 (Fig. 5A, B), further supporting a decisive role of ATX/LPA in HSC activation. In agreement, LPA stimulation of serum starved primary HSCs *in vitro* stimulated aSMA expression (Fig. 5C), while promoting the rearrangement of their actin cytoskeleton, and inhibiting their serum-starvation-induced apoptosis (Fig. 5 D,E respectively).

Pharmacological inhibition of ATX attenuates CCl_4-induced fibrosis. To translate the genetic findings into potential treatment options, CCl_4-treated mice were administered (2-4w post CCl_4) with 30 mg/Kg (IP, bid) PF8380, a potent (IC50 1.9

nM) and well characterized[17,18] ATX inhibitor. Pharmacologic ATX inhibition attenuated CCl_4-induced fibrosis (Fig. 6A-F), confirming the genetic results and suggesting ATX as a potential therapeutic target in liver fibrosis.

Hepatocyte-specific ATX genetic deletion attenuates HCC development. To examine a possible role of ATX/LPA pro-fibrotic effects in HCC development, male *AlbEnpp2*$^{-/-}$ mice were administered, prior to CCl_4 intoxication and the observed effects in liver pathophysiology and ATX expression, with DEN (50 mg/Kg; IP at 15 days postpartum), thus coupling a genotoxic mutagenic insult with toxin-induced fibrosis that results to HCC.[19]

All DEN/CCl_4-treated, surviving (60%; Fig. 7A) control mice developed HCC (Fig. 7B). Among them, the majority (70%) developed tumours in all the liver lobes; in the remaining mice, tumorigenesis confined to the caudate lobes and left lateral lobes (Fig. S11A). Increased ATX mRNA levels were detected upon HCC development (Fig. 7C); no changes in ATX plasma activity were observed (Fig. S11B). ATX staining localized in tumour cells, missing from healthy surrounding Heps (Fig. S11C).

ATX genetic deletion attenuated ATX mRNA and plasma activity levels (Figs. 7C and S11B respectively); however, residual ATX staining in remaining tumours could still be detected (Fig. S11C), most likely as a result of not complete (<100%) recombination and/or possible ATX attachment to membrane receptors such as integrins.[20,21] All (100%) DEN/CCl_4-treated *AlbEnpp2*$^{-/-}$ mice survived the treatment (Fig. 7A); among them, 30% did not develop any tumours and 45% developed tumours only in some liver lobes (caudate lobes and left lateral lobe; Figs. 7B and S11A), suggesting that ATX/LPA amplify oncogenic signals. The dramatic reduction

of both tumour number and size (Fig. 7D,E) was also reflected in liver weight (Fig. S11D). Histological analysis indicated a reduction trend in necrosis, inflammation and fibrosis (Fig. S12A-D), and a significant decrease in CD34 and PCNA staining (Fig. S12E-H); however, the most prominent histological feature observed upon the genetic deletion of ATX was a significant decrease of neutral lipid deposition (Fig. 7F).

ATX distorts HCC fatty acid (FA) metabolism. Lipidomic analysis indicated upregulated levels of liver LPA upon HCC development, found diminished upon the genetic deletion of ATX (Fig. 2E and S11F). Noteworthy, *Ppap2b* mRNA levels were found decreased also in HCC (Fig. S11G), as shown (Table S1B) for human HCC patients, possibly accounting for the sustainment of LPA levels. Although PPAP2s have been also incriminated for S1P degradation,[22] no major differences in S1P levels were observed in HCC (Fig. S11H); however, large increases in the expression of *S1pr3* were observed upon HCC development, found diminished after the ablation of ATX and LPA (Fig. S11K, Table S5), in agreement with previous *in vitro* studies.[23]

Strikingly, liver accumulation of some TAG species in DEN/CCl_4-induced HCC was the most prominent feature of the HCC lipidomic profile (Fig. 2E); HCC TAG levels were found reduced in the absence of ATX, in agreement with the observed decreased neutral lipid deposition, suggesting a novel role for ATX/LPA in HCC-related FA metabolism.

To obtain mechanistic insights into the mode of action of the ATX/LPA axis in HCC development, we performed whole liver, genome wide expression profiling of DEN/CCl_4-induced HCC. Stringent gene set enrichment analysis of statistical significant differentially expressed genes (DEGs) upon HCC development in the absence of ATX identified mostly genes involved in lipid metabolism, as well as

genes coding for plasma membrane and actin binding proteins (Table S4). The expression of a large number of ATX/LPA affected genes seem to be regulated by the transcription factor AP-1 (Table S4), a critical transcriptional regulator of invasion[24] previously reported to be regulated by LPA.[5]

Comparison of $HCC^{\Delta ATX}$ and HCC DEGs revealed genes that are upregulated in the liver upon HCC development but reverted towards physiological levels in the absence of ATX (Table S5). The HCC-induced, possibly ATX/LPA-regulated genes (ATX-rDEGs; Table S5) include *Afp* and *Gpc3*, established HCC serum markers,[25] as well as well-known markers of oncofetal transformation (*Afp*, *H19*, *Bex-1*),[19,26] proving on a molecular level that ATX deletion attenuates HCC.

Among the multiple ATX-rDEGs involved in lipid metabolism, stearoyl-CoA desaturase 2 (*Scd2*) was previously shown to be necessary for the biosynthesis of monounsaturated FA, essential components of TAGs.[27] DEN/CCl_4-mediated HCC development induced its expression, whereas ATX deletion attenuated its mRNA levels (Table S5, confirmed with Q-RT-PCR, Fig. 8A). In agreement, LPA stimulation of HepG2 cells *in vitro* stimulated *SCD* mRNA expression (Fig. 8B), neutral lipid deposition (Fig. 8C,D) and cellular TAG levels (as determined with LC/MS; Fig. 8E).

Discussion

Increased ATX sera levels were detected in CLD patients of different etiologies, associated with shorter overall survival and surrogate disease parameters indicative of hepatic damage and loss of function (Table S3).[28]. Moreover, increased liver ATX mRNA expression was found in the majority of publically available CLD and HCC microarray datasets, thus proving that hepatocyte injury can stimulate autologous ATX expression and suggesting that ATX, beyond its diagnostic or prognostic value, might also play a direct role in liver pathophysiology.

In agreement, robust ATX and LPA expression was detected in CCl_4 intoxicated mouse livers. ATX expression was localized mainly to hepatocytes, found to be induced by HCV infection, TNF-mediated inflammation, as well as exposure to LPC, all pathological stimuli linked with the development of different forms of human CLDs. Interestingly, TNF has been reported to stimulate ATX expression in hepatoma cells *in vitro* via NF-κB,[29] while LPS, a well-known activator of NF-kB in macrophage-like cells,[30] has also been shown to induce ATX expression in monocytic THP-1 cells,[31] as shown here with primary kupffer cells. LPC has been also shown to activate NF-kB in keratinocytes and pancreatic AR42J cells,[32,33] while the activation of NF-kB is well established in HCV infections.[30] Moreover, *in silico* analysis of the *Ennp2* promoter revealed NF-kB target sites, validated by the respective ChIPs,[34] strongly suggesting that ATX expression in the inflamed liver is controlled, at least in part, by NF-kB, which had been suggested to link injury, fibrosis and HCC, depending on cellular context and timing, as well as on activation thresholds.[30]

Hepatocyte ATX expression and LPA production in CCl_4 intoxicated mouse livers coincided with a proliferative peak of hepatocytes, although no major effect of ATX/LPA in hepatocyte proliferation was observed *in vitro*, or in hepatectomized

mice *in vivo*. Moreover, hepatocyte-specific ATX deletion and the consequent reduction in local LPA levels attenuated neutral lipid deposition. In agreement and as recently presented,[35] hepatocyte-specific ATX deletion abrogated lipid deposition in the liver and the development of steatosis in a more relevant, high fat diet-induced NASH metabolic model, associated with reduced expression of major lipogenic genes. However, the relative contribution of ATX/LPA to FA synthesis and TAG deposition in comparison with other converging pathways, as well as exogenous FA sources, remains to be determined.

On the other hand and most importantly, ATX expression also coincided with upregulated aSMA protein expression, *Cyp2S1* mRNA expression and RA levels, all established markers of HSC activation.[36] Deletion or overexpression of ATX from hepatocytes modulated accordingly aSMA levels in all disease models examined, while exposure of primary HSCs to LPA promoted cytoskeletal rearrangements, inhibited apoptosis and stimulated aSMA expression. Moreover, ATX well-timed expression coincided with the transition from regeneration to fibrosis, as shown with a major shift in the expression ratio of *Cxcr4*/*Cxcr7*, a recently reported modelled disease hallmark.[37] This predominance of CXCR4 over CXCR7 is thought to shift the angiocrine response of liver sinusoidal endothelial cells, recently shown that can be modulated by LPA,[38] stimulating proliferation of HSCs and enforcing a pro-fibrotic vascular niche.[37] Therefore, CCl_4-induced and LPC-driven, hepatocyte ATX expression enforces the entry to the perpetuation phase of fibrosis development by activating HSCs, directly or indirectly, through LPA, whose levels are possibly sustained in relatively high levels due to the downregulation of *Ppap2b* expression, further stimulating collagen production and hepatic fibrosis.

LPC, the main enzymatic substrate of ATX and a potent inducer of its Hep expression, peaked at 4w post CCl_4 in liver tissue, as also suggested for NAFLD patients[39]. Moreover, LPC administration has been reported to promote hepatitis[39]; interestingly, rats fed a high fat diet displayed elevated serum ALT levels that correlated with increased *Pla2* mRNA expression and LPC levels[40], suggesting that LPC and ATX/LPA could mediate diet and/or obesity effects in liver pathophysiology, as previously suggested for prostate disease[41]. Different PLA2 isoforms were detected aberrantly expressed in mouse and human fibrotic livers, further supporting liver specific de novo LPC synthesis upon damage, and suggesting a synergy of the PLA2/LPC and LPA/ATX axes in hepatitis development[42].

Conditional genetic deletion of ATX from Heps and abrogation of liver production of LPA modulated inflammation and diminished fibrosis, thus establishing ATX as a liver pro-fibrotic factor. Conversely, transgenic Heps-ATX overexpression promoted collagen deposition and fibrosis; noteworthy, the transgenic liver ATX expression did not induce any liver phenotype *per se*, suggesting that ATX expression is not sufficient to induce fibrosis, but is rather required to amplify pro-fibrotic signals.

Deletion of ATX from Heps and downregulation of liver LPA levels had also a profound effect in DEN/CCl_4-induced HCC, promoting mice survival and attenuating both liver tumor numbers and size. In agreement with a pro-carcinogenic role for ATX, transgenic overexpression of ATX in the mammary gland resulted to spontaneous breast cancer in aged mice;[43] noteworthy, the late onset suggests that ATX is not sufficient to promote carcinogenesis *per se*, as shown here for fibrosis, but is rather required to amplify oncogenic age-related signals. Moreover, reported LPA effects *in vitro* are concordant with several of the suggested hallmarks of cancer, a

conceptual framework of essential alterations in cell physiology that collectively dictate malignant growth in most tumors[44]. LPA effects, mediated by pathways well consistent with their identity as GPCRs, include proliferation, resistance to cell death, angiogenesis, as well as invasion and metastasis[5].

Cancer cells, under the pressure of increased proliferation and growth, have been suggested to reprogram their cellular energy metabolism in many different ways, including an increase in glutamine metabolism, the decoupling of glycolysis from pyruvate oxidation in mitochondria (the Warburg effect) and *de novo* FA synthesis, despite sufficient dietary supply and/or increased lipolysis in the adipose tissue.[44,45] Excessive FAs, that can be detrimental for the cell, are esterified with glycerol backbones generating TAGs that are stored in lipid droplets.[44,45] At times of metabolic need such as malignant growth, accumulated TAGs can be converted back to FAs through emerging lipolytic mechanisms that were also reported to be upregulated in cancer.[44,45] Although this delicate balance of FA metabolism in cancer is far from being understood, FAs are essential to cancer cells for the synthesis of structural lipids required for the generation of new cells and the required energy production to sustain it, the biosynthesis of pro-tumorigenic signaling lipids, as well as the resistance to oxidative stress-induced cell death and chemotherapy.[44,45]

Strikingly, the most prominent histopathological effect of ATX deletion in DEN/CCl_4-induced HCC was the significant decrease of neutral lipid deposition, indicating perturbations in FA metabolism; no significant liver accumulation of TAGs was detected upon the genetic deletion of ATX, while expression profiling revealed as mostly affected, genes that are involved in lipid metabolism. Among them, *Scd2* expression, essential for FA synthesis during early liver development,[27] was shown to be aberrantly re-activated in DEN/CCl_4-induced HCC, and was found to be stimulated

by LPA *in vitro* correlating with increased TAG accumulation. In support, *Scd2* expression has been shown to be regulated by sterol regulatory element-binding proteins (SREBP 1a and 2),[46] transcription factors regulating FA synthesis[46] and previously shown to be stimulated by LPA.[47] Pharmacological inhibition of SCD, as well as of other enzymes involved in FA synthesis, have been reported to reduce tumor growth and are currently at different levels of preclinical and clinical development.[45] Noteworthy, ATX/LPA also stimulated the expression of a large number of lipase genes (Tables S4 and S5), such as Patatin like phospholipase domain containing 5 (PNPLA5; Table S5) a neutral lipase that localizes to lipid droplets and has been shown as a link of TAG mobilization and autophagy.[48] Therefore, the ATX/LPA axis is critically involved in FA metabolism in cancer cells, in concert with other lipid modifying enzymatic cascades and likely orchestrated from the adipose tissue, thus contributing to the reprogramming of energy metabolism in malignant cells, an emerging and maybe central cancer hallmark.

Pharmacological inhibition of ATX with Pfizer's PF8380 attenuated CCl_4-induced fibrosis, in agreement with the genetic deletion results. Noteworthy, ATX was recently reported to be inhibited by the selective binding of the bile salt taurourdeoxycholate (TUDCA),[49] an established treatment of primary biliary cirrhosis and other cholestatic disorders, suggesting that TUDCA efficacy could be partly attributed to ATX inhibition. Therefore, ATX emerges as a potential therapeutic target in CLDs and possibly HCC, perhaps as an adjuvant therapy to current treatment options.

Author contributions

EK performed the majority of presented experiments. AK and IN performed Q-RT-PCRs and MZ ATX WB/IHCs. EK, AK and IN analysed and quantified pathology findings, confirmed by EK and VG. NX performed data mining of microarray datasets. VH produced and analysed microarray data. PF, AD and UG performed the HCV *in vitro* studies. ANM quantified RA levels. GND provided patient samples and their demographic, clinical and laboratory data. EK and VA designed the experiments and wrote the paper.

Acknowledgements

We would like to thank T. Chavakis and I. Talianidis for critical reading of the manuscript. The Tg*a1t1Ennp2* transgenic mouse and the PF8380 compound were kindly provided by G. Mills and F. Hoffmann-La Roche Ltd respectively.

References

1. Friedman SL. Evolving challenges in hepatic fibrosis. Nat Rev Gastroenterol Hepatol 2010;7:425-436.

2. Aikawa S, Hashimoto T, Kano K, Aoki J. Lysophosphatidic acid as a lipid mediator with multiple biological actions. J Biochem 2015;157:81-89.

3. Choi JW, Herr DR, Noguchi K, Yung YC, Lee CW, Mutoh T, Lin ME, et al. LPA receptors: subtypes and biological actions. Annu Rev Pharmacol Toxicol 2010;50:157-186.

4. Benesch MG, Ko YM, McMullen TP, Brindley DN. Autotaxin in the crosshairs: Taking aim at cancer and other inflammatory conditions. FEBS Lett 2014;588:2712-2727.

5. Barbayianni E, Kaffe E, Aidinis V, Kokotos G. Autotaxin, a secreted lysophospholipase D, as a promising therapeutic target in chronic inflammation and cancer. Prog Lipid Res 2015;58:76-96.

6. Oikonomou N, Mouratis MA, Tzouvelekis A, Kaffe E, Valavanis C, Vilaras G, Karameris A, et al. Pulmonary autotaxin expression contributes to the pathogenesis of pulmonary fibrosis. Am J Respir Cell Mol Biol 2012;47:566-574.

7. Ikeda H, Yatomi Y. Autotaxin in liver fibrosis. Clin Chim Acta 2012;413:1817-1821.

8. Fotopoulou S, Oikonomou N, Grigorieva E, Nikitopoulou I, Paparountas T, Thanassopoulou A, Zhao Z, et al. ATX expression and LPA signalling are vital for the development of the nervous system. Dev Biol 2010;339:451-464.

9. Postic C, Magnuson MA. DNA excision in liver by an albumin-Cre transgene occurs progressively with age. Genesis 2000;26:149-150.

10. Soriano P. Generalized lacZ expression with the ROSA26 Cre reporter strain. Nat Genet 1999;21:70-71.

11. Pamuklar Z, Federico L, Liu S, Umezu-Goto M, Dong A, Panchatcharam M, Fulkerson Z, et al. Autotaxin/lysopholipase D and Lysophosphatidic Acid Regulate Murine Hemostasis and Thrombosis. J Biol Chem 2009;284 7385-7394.

12. Mazzocca A, Dituri F, De Santis F, Filannino A, Lopane C, Betz RC, Li YY, et al. Lysophosphatidic acid receptor LPAR6 supports the tumorigenicity of hepatocellular carcinoma. Cancer Res 2015;75:532-543.

13. Brindley DN, Pilquil C. Lipid phosphate phosphatases and signaling. J Lipid Res 2009;50 Suppl:S225-230.

14. Mizuhara H, O'Neill E, Seki N, Ogawa T, Kusunoki C, Otsuka K, Satoh S, et al. T cell activation-associated hepatic injury: mediation by tumor necrosis factors and protection by interleukin 6. J Exp Med 1994;179:1529-1537.

15. Benesch MG, Zhao YY, Curtis JM, McMullen TP, Brindley DN. Regulation of autotaxin expression and secretion by lysophosphatidate and sphingosine 1-phosphate. J Lipid Res 2015;56:1134-1144.

16. Chemin J, Patel A, Duprat F, Zanzouri M, Lazdunski M, Honore E. Lysophosphatidic acid-operated K+ channels. J Biol Chem 2005;280:4415-4421.

17. Gierse JK, Thorarensen A, Beltey K, Bradshaw-Pierce E, Cortes-Burgos L, Hall T, Johnston A, et al. A Novel Autotaxin Inhibitor Reduces Lysophosphatidic Acid Levels in Plasma and the Site of Inflammation. J Pharmacol Exp Ther 2010;334:310-317.

18. Katsifa A, Kaffe E, Nikolaidou-Katsaridou N, Economides AN, Newbigging S, McKerlie C, Aidinis V. The Bulk of Autotaxin Activity Is Dispensable for Adult Mouse Life. PLoS One 2015;10:e0143083.

19. Dapito DH, Mencin A, Gwak GY, Pradere JP, Jang MK, Mederacke I, Caviglia JM, et al. Promotion of hepatocellular carcinoma by the intestinal microbiota and TLR4. Cancer Cell 2012;21:504-516.

20. Hausmann J, Kamtekar S, Christodoulou E, Day JE, Wu T, Fulkerson Z, Albers HM, et al. Structural basis of substrate discrimination and integrin binding by autotaxin. Nat Struct Mol Biol 2011;18:198-204.

21. Leblanc R, Lee SC, David M, Bordet JC, Norman DD, Patil R, Miller D, et al. Interaction of platelet-derived autotaxin with tumor integrin alphaVbeta3 controls metastasis of breast cancer cells to bone. Blood 2014.

22. Tang X, Zhao YY, Dewald J, Curtis JM, Brindley DN. Tetracyclines increase lipid phosphate phosphatase expression on plasma membranes and turnover of plasma lysophosphatidate. Journal of Lipid Research 2016;57:597-606.

23. Ptaszynska MM, Pendrak ML, Stracke ML, Roberts DD. Autotaxin signaling via lysophosphatidic acid receptors contributes to vascular endothelial growth factor-induced endothelial cell migration. Mol Cancer Res 2010;8:309-321.

24. Ozanne BW, Spence HJ, McGarry LC, Hennigan RF. Transcription factors control invasion: AP-1 the first among equals. Oncogene 2007;26:1-10.

25. Bertino G, Ardiri A, Malaguarnera M, Malaguarnera G, Bertino N, Calvagno GS. Hepatocellualar carcinoma serum markers. Semin Oncol 2012;39:410-433.

26. Uehara T, Ainslie GR, Kutanzi K, Pogribny IP, Muskhelishvili L, Izawa T, Yamate J, et al. Molecular mechanisms of fibrosis-associated promotion of liver carcinogenesis. Toxicol Sci 2013;132:53-63.

27. Miyazaki M, Dobrzyn A, Elias PM, Ntambi JM. Stearoyl-CoA desaturase-2 gene expression is required for lipid synthesis during early skin and liver development. Proc Natl Acad Sci U S A 2005;102:12501-12506.

28. Pleli T, Martin D, Kronenberger B, Brunner F, Koberle V, Grammatikos G, Farnik H, et al. Serum autotaxin is a parameter for the severity of liver cirrhosis and overall survival in patients with liver cirrhosis--a prospective cohort study. PLoS One 2014;9:e103532.

29. Wu JM, Xu Y, Skill NJ, Sheng H, Zhao Z, Yu M, Saxena R, et al. Autotaxin expression and its connection with the TNF-alpha-NF-kappaB axis in human hepatocellular carcinoma. Mol Cancer 2010;9:71.

30. Luedde T, Schwabe RF. NF-kappaB in the liver--linking injury, fibrosis and hepatocellular carcinoma. Nat Rev Gastroenterol Hepatol 2011;8:108-118.

31. Li S, Zhang J. Lipopolysaccharide induces autotaxin expression in human monocytic THP-1 cells. Biochem Biophys Res Commun 2009;378:264-268.

32. Masamune A, Sakai Y, Yoshida M, Satoh A, Satoh K, Shimosegawa T. Lysophosphatidylcholine Activates Transcription Factor NF-κB and AP-1 in AR42J Cells. Digestive Diseases and Sciences 2001;46:1871-1881.

33. Ryborg AK, Johansen C, Iversen L, Kragballe K. Lysophosphatidylcholine induces keratinocyte differentiation and upregulation of AP-1- and NF-kappaB DNA-binding activity. Acta Derm Venereol 2004;84:433-438.

34. Lovas A, Weidemann A, Albrecht D, Wiechert L, Weih D, Weih F. p100 Deficiency is insufficient for full activation of the alternative NF-kappaB pathway: TNF cooperates with p52-RelB in target gene transcription. PLoS One 2012;7:e42741.

35. Subramanian P, Techritz N, Prucnal M, Aidinis V, Chavakis T. Cell type-specific role of ATX in nonalcoholic steatohepatitis (NASH). 13th International Conference on Innate Immunity, 23-28/06/2016, Rhodes, Greece 2016;P72.

36. D'Ambrosio DN, Walewski JL, Clugston RD, Berk PD, Rippe RA, Blaner WS. Distinct populations of hepatic stellate cells in the mouse liver have different capacities for retinoid and lipid storage. PLoS One 2011;6:e24993.

37. Ding BS, Cao Z, Lis R, Nolan DJ, Guo P, Simons M, Penfold ME, et al. Divergent angiocrine signals from vascular niche balance liver regeneration and fibrosis. Nature 2014;505:97-102.

38. Chou CH, Lai SL, Ho CM, Lin WH, Chen CN, Lee PH, Peng FC, et al. Lysophosphatidic acid alters the expression profiles of angiogenic factors, cytokines, and chemokines in mouse liver sinusoidal endothelial cells. PLoS One 2015;10:e0122060.

39. Han MS, Park SY, Shinzawa K, Kim S, Chung KW, Lee JH, Kwon CH, et al. Lysophosphatidylcholine as a death effector in the lipoapoptosis of hepatocytes. J Lipid Res 2008;49:84-97.

40. Huang Y, Fu JF, Shi HB, Liu LR. Metformin prevents non-alcoholic fatty liver disease in rats: role of phospholipase A2/lysophosphatidylcholine lipoapoptosis pathway in hepatocytes. Zhonghua Er Ke Za Zhi 2011;49:139-145.

41. Kulkarni P, Getzenberg RH. High-fat diet, obesity and prostate disease: the ATX-LPA axis? Nat Clin Pract Urol 2009;6:128-131.

42. Sevastou I, Kaffe E, Mouratis MA, Aidinis V. Lysoglycerophospholipids in chronic inflammatory disorders: The PLA(2)/LPC and ATX/LPA axes. Biochimica et biophysica acta 2013;1831:42-60.

43. Liu S, Umezu-Goto M, Murph M, Lu Y, Liu W, Zhang F, Yu S, et al. Expression of autotaxin and lysophosphatidic acid receptors increases mammary tumorigenesis, invasion, and metastases. Cancer Cell 2009;15:539-550.

44. Hanahan D, Weinberg Robert A. Hallmarks of Cancer: The Next Generation. Cell 2014;144:646-674.

45. Rohrig F, Schulze A. The multifaceted roles of fatty acid synthesis in cancer. Nat Rev Cancer 2016.

46. Shimomura I, Shimano H, Korn BS, Bashmakov Y, Horton JD. Nuclear sterol regulatory element-binding proteins activate genes responsible for the entire program of unsaturated fatty acid biosynthesis in transgenic mouse liver. J Biol Chem 1998;273:35299-35306.

47. Mukherjee A, Wu J, Barbour S, Fang X. Lysophosphatidic acid activates lipogenic pathways and de novo lipid synthesis in ovarian cancer cells. J Biol Chem 2012;287:24990-25000.

48. Dupont N, Chauhan S, Arko-Mensah J, Castillo EF, Masedunskas A, Weigert R, Robenek H, et al. Neutral lipid stores and lipase PNPLA5 contribute to autophagosome biogenesis. Curr Biol 2014;24:609-620.

49. Keune WJ, Hausmann J, Bolier R, Tolenaars D, Kremer A, Heidebrecht T, Joosten RP, et al. Steroid binding to Autotaxin links bile salts and lysophosphatidic acid signalling. Nat Commun 2016;7:11248.

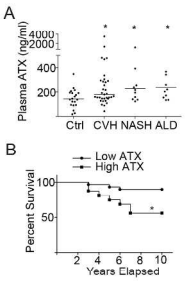

210x297mm (300 x 300 DPI)

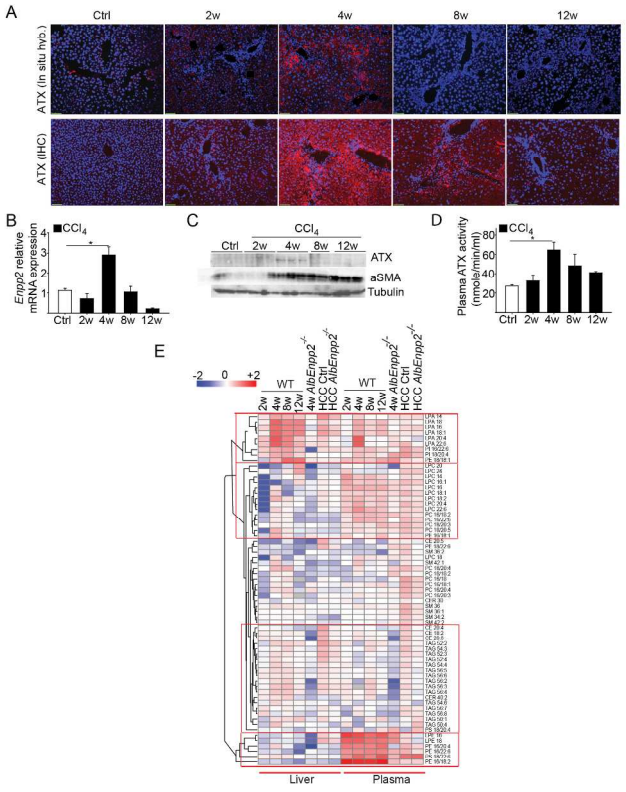

210x297mm (300 x 300 DPI)

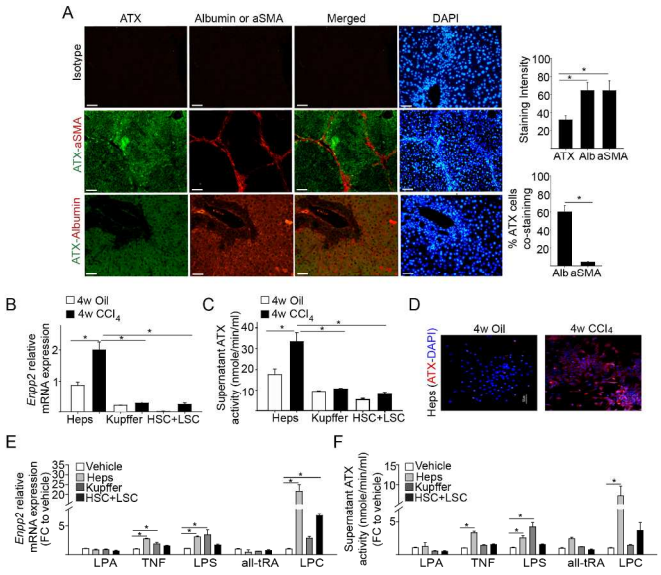

210x297mm (300 x 300 DPI)

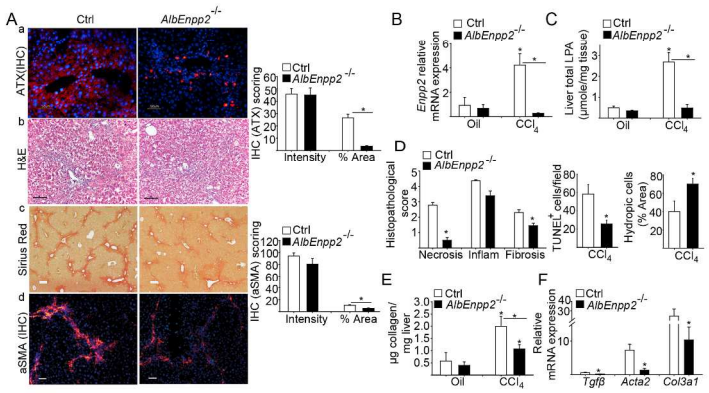

210x297mm (300 x 300 DPI)

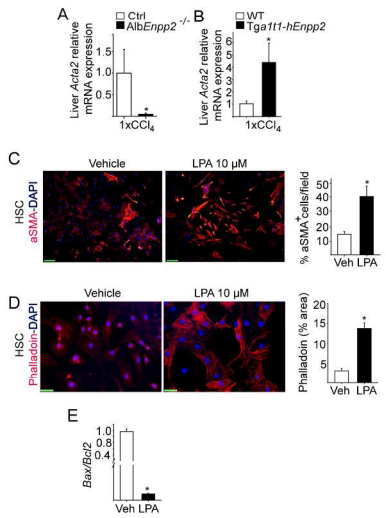

210x297mm (300 x 300 DPI)

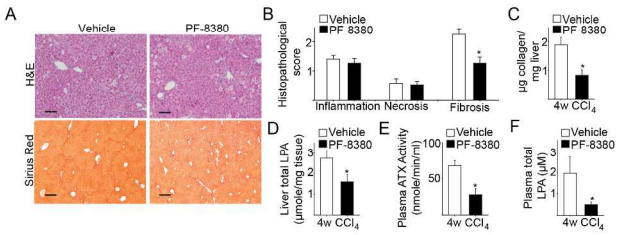

210x297mm (300 x 300 DPI)

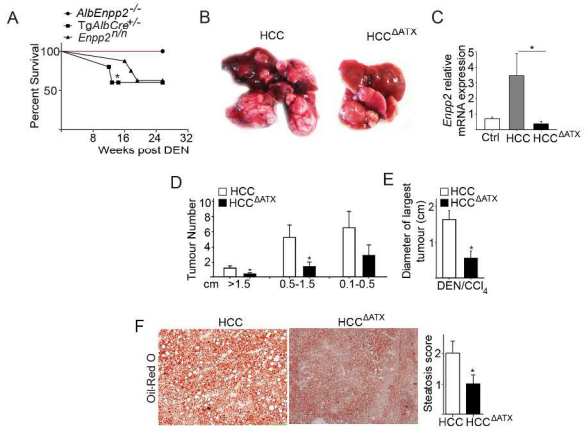

210x297mm (300 x 300 DPI)

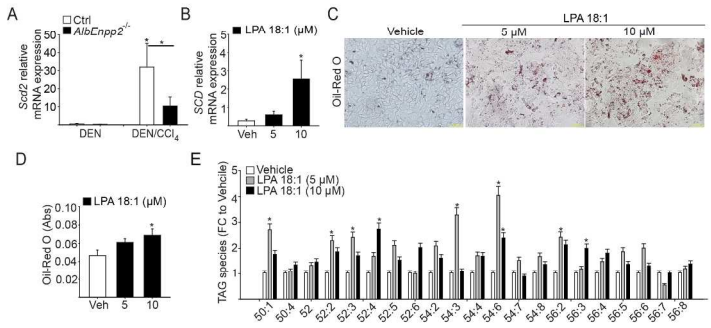

210x297mm (300 x 300 DPI)

Figure legends

Fig. 1. Increased serum ATX levels in CLD patients of different etiologies, correlating with poor survival. (A) ATX serum levels in CVH (n=35), NASH (n=12), and ALD (n=12) patients, as measured with ELISA, in comparison to healthy controls (n=20). Median values are shown; *p<0.05 to control values; Mann Whitney test. (B) High ATX levels (2 fold higher than the normal values) are associated with poor cumulative survival, in a Kaplan-Meier survival curve. n=59; *p<0.05, Log-rank (Mantel-Cox) test.

Fig. 2. Chronic CCl_4 intoxication stimulates ATX expression and distorts lipid homeostasis. (A) *In situ* hybridization with an ATX antisense probe and IHC with an a-ATX monoclonal antibody (7A5) in liver sections at the indicated time points post CCl_4 administration in WT mice. Sections were counterstained with DAPI (in blue). (B) Q-RT-PCR analysis for ATX (*Enpp2*) mRNA expression in liver extracts at the indicated time points of the same mice. (C) Western blot in liver extracts for ATX, aSMA and Tubulin as loading control. (D) Plasma ATX activity as measured with the TOOS assay. (E) Lipidomic analysis with HPLC-ESI/MS/MS of liver tissue and plasma samples at 2-12w post CCl_4 administration in WT mice. The heatmap includes for direct comparison purposes, the corresponding lipid profiles from CCl_4-treated, as well as DEN/CCl_4-treated (HCC), *AlbEnpp2*$^{-/-}$ mice. Fold changes to the respective littermate oil-treated control values are shown; clustering was performed using the Euclidean's distance metrics. All values in all panels are mean +/- SEM; n=4-6. *p<0.05; ANOVA post hoc test. Scale bars: 150μm.

Fig. 3. Hepatocyte specific ATX expression is stimulated by a variety of liver pathogenic stimuli. (A) Representative double IHC staining for ATX and albumin or aSMA in liver sections, counterstained with DAPI, 4w post CCl_4 administration and the relative quantifications. (B, E) Q-RT-PCR analysis for ATX (*Enpp2)* relative mRNA expression in primary liver cells *ex vivo*. (C, F) ATX activity, as measured with the TOOS assay, in the supernatants of the cells shown in B/E respectively. (D) Representative IHC for ATX in the indicated cultured hepatocytes. All values are mean +/- SEM; n=3-6; *p<0.05; ANOVA post hoc test. Scale bar: 50μm.

Fig. 4. Hepatocyte-specific ATX genetic deletion ameliorates CCl_4-induced liver fibrosis. (Aa-d) Representative staining images of liver sections 4w post CCl_4 administration in *AlbEnpp2*$^{-/-}$ and control (Ctrl; Tg*Alb-Cre*) littermate mice. Scale bars: 50 μm: a; 100 μm: d; 150 μm: b; 200 μm: c. (B) Q-RT-PCR analysis for ATX (*Enpp2*) relative mRNA expression in the indicated liver extracts. (C) Liver total LPA levels, as determined with HPLC-ESI/MS/MS. (D) Semi-quantitative scoring of necrosis, apoptosis ($TUNEL^+$ cells), hydropic cells, inflammation and fibrosis at the indicated mice at 4w post CCl_4 administration. (E) Liver collagen deposition was quantified by hydroxyproline levels (F) Q-RT-PCR analysis of pro-fibrotic gene expression in liver extracts. Q-RT-PCR arbitrary (ΔΔCt) values were normalized to the expression levels of *B2m* in the same samples and presented as fold change to control values (oil treated mice). Blind evaluation of all histology scoring was performed from 2 reviewers and confirmed by 2 independent expert pathologists. All values are mean +/- SEM; n=3-9. *p<0.05 to the respective control or indicated values; Unpaired, two-sided Student's t-test, or Mann-Whitney test for non-normal distributions.

Fig. 5. ATX/LPA promote HSCs activation. (A) Hepatocyte-specific genetic deletion in *AlbEnpp2*$^{-/-}$ mice decreases *Acta2* liver mRNA expression, while (B) transgenic overexpression of ATX in Tg*a1t1-hEnpp2* mice increases it, 24h post-acute exposure to CCl_4, as determined with Q-RT-PCR analysis; n=5-12. (C) Representative aSMA staining images of serum-starved, LPA-stimulated mouse primary HSCs *ex vivo*, and respective quantification. (D) Representative images of F-actin (phalloidin) staining in the same cells and respective quantification (E) Q-RT-PCR analysis of *Bax/Bcl-2* mRNA expression, as determined with Q-

RT-PCR; n=3. Q-RT-PCR arbitrary (ΔΔCt) values were normalized to the expression levels of *B2m* in the same samples and presented as fold change to control values. All values are mean +/- SEM; *p<0.05 to respective control values; unpaired, two sided Student's t-test; scale bars: 60 μm (C) and 30 μm (E).

Fig. 6. Pharmacological ATX inhibition attenuates CCl_4-induced fibrosis. (A) Representative H&E and sirius red staining (scale bars 100 and 200 μm respectively) in liver sections 4w post CCl_4 administration in WT mice treated (2-4w) with PF8380 or vehicle-treated littermates. (B) Semi-quantitative scoring of inflammation, necrosis and fibrosis in liver sections of the same mice. (C) Liver collagen deposition in the livers was quantified by hydroxyproline levels. (D, F) Liver/plasma total LPA levels as measured with HPLC-ESI-MS/MS. (E) Plasma ATX activity measured with TOOS in the same mice. Blind evaluation of all histology scoring was performed from 2 reviewers and confirmed by 2 independent expert pathologists. All values are mean +/- SEM; n=5-7. *p<0.05 to vehicle values; unpaired, two-sided Student's t-test or Mann-Whitney test for non-normal distributions.

Fig. 7. Hepatocyte specific deletion of ATX attenuates HCC development. (A) The genetic deletion of ATX from hepatocytes significantly improves survival upon DEN/CCl_4 treatment. n=4-14; Gehan-Breslow-Wilcoxon test. (B) Macroscopic liver appearance of DEN/CCl_4-treated *AlbEnpp2*$^{-/-}$ ($HCC^{\Delta ATX}$) or control *Enpp2* $^{n/n}$ littermate mice (HCC). (C) Q-RT-PCR analysis of relative *Enpp2* mRNA expression in the indicated mouse strains. (D) Tumor number and (E) average size of the largest tumor in the presence or absence of hepatocyte ATX expression. (F) Representative Oil Red-O staining of liver sections (Scale bar 150 μm) in the same mice and respective quantification. All values are mean +/- SEM. n=7-12. *p<0.05 to respective control or indicated values; unpaired, two-sided Student's t-test or Mann-Whitney for non-normal distributions.

Fig. 8. LPA stimulates *SCD* mRNA expression and TAG accumulation in Hep2G cells *in vitro*. (A) Q-RT-PCR analysis of *Scd2* relative liver mRNA expression in the indicated mouse strains and treatments. Ctrl are the littermate controls of *AlbEnpp2*$^{-/-}$ (B) Q-RT-PCR analysis of *SCD* mRNA expression in serum-starved, LPA-stimulated Hep2G cells *in vitro*. Q-RT-PCR arbitrary (ΔΔCt) values were normalized to the expression levels of *B2m* in the same samples and presented as fold change to vehicle. (C) Representative Oil-Red O staining of the same cells; scale bar: 150 μm. (D) Independent quantification of neutral lipids content of the same cells with a colorimetric method. (E) The TAG content of LPA-treated Hep2G cells *in vitro*, as determined with HPLC-ESI/MS/MS, presented as fold change to control values (vehicle). All values are mean +/- SEM. n=3-4. *p<0.05 to the respective control or indicated values; unpaired, two-sided Student's t-test or Mann-Whitney for non-normal distributions.

.

Hepatocyte Autotaxin expression promotes liver fibrosis and cancer

Eleanna Kaffe[1], Aggeliki Katsifa[1], Nikos Xylourgidis[1], Ioanna Ninou[1], Markella Zannikou[1], Vaggelis Harokopos[1], Pelagia Foka[2], Alexios Dimitriadis[2], Kostas Evangelou[3], Anargyros N. Moulas[4], Urania Georgopoulou[2], Vassilis G. Gorgoulis[3,5,6], George N. Dalekos[7] and Vassilis Aidinis[1]

Supporting Information

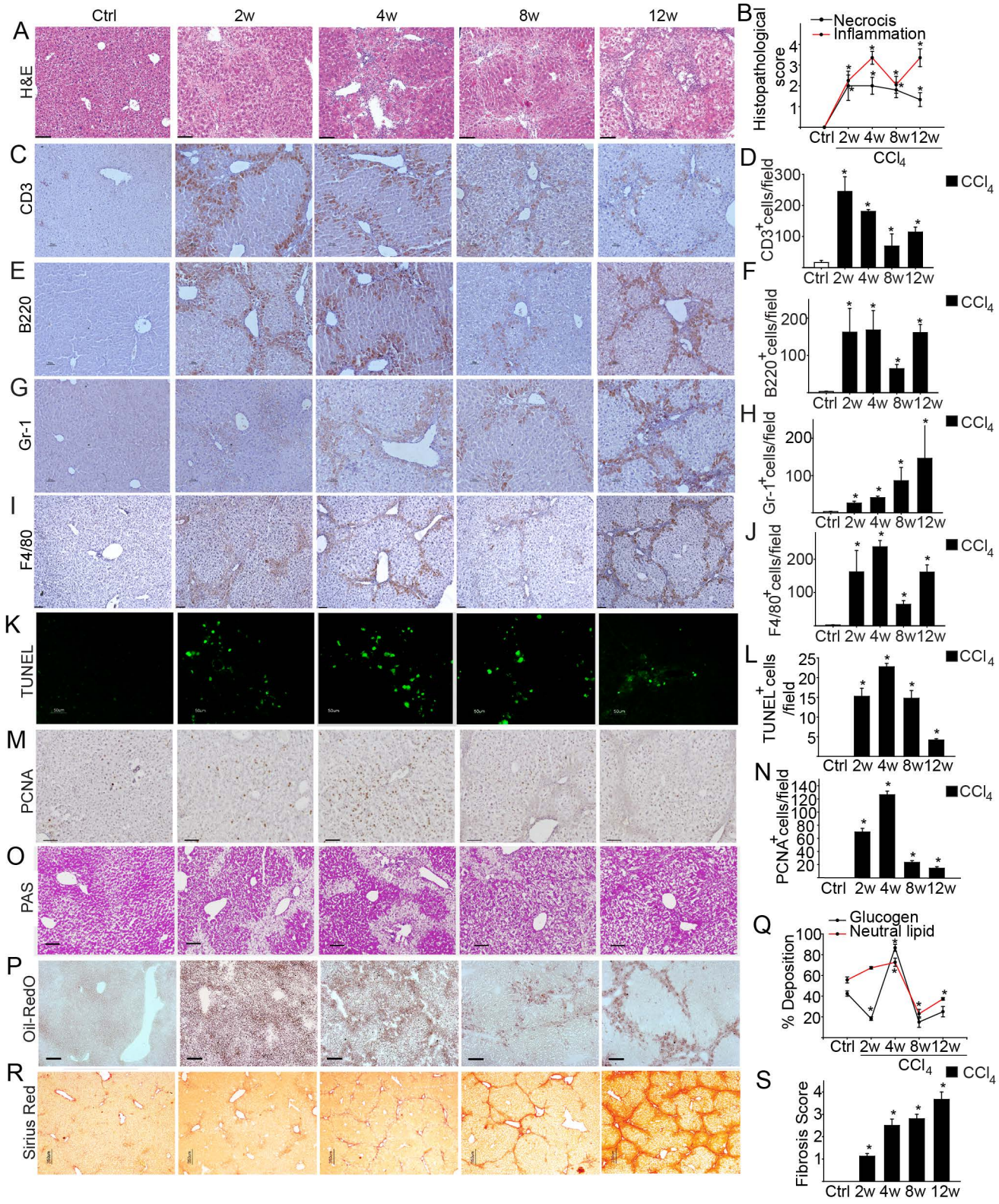

Fig. S1. Detailed pathology evaluation of disease development upon chronic CCl_4 intoxication reveals increased damage, accompanied by infiltration of different cell types, apoptosis, proliferation, glycogen and neutral lipid deposition leading to progressive liver fibrosis. (**A-S**) Representative images from liver sections stained as indicated for H&E, for the indicate inflammatory cell markers, for apoptosis (TUNEL), proliferation (PCNA-IHC), glucogen (Periodic-acid shiff stain; PAS), neutral lipids (Oil-Red O), fibrosis (Sirius red) at different time points post CCl_4 administration in WT mice. Ctrl littermate mice were treated with just oil. Blind evaluation of all histology scoring was performed from 3 reviewers and confirmed by 2 independent expert pathologists. All values in graphs are mean +/- SEM; n=4-6; *p<0.05 to control (oil treated mice) values; unpaired Student's t-test, two sided. Scale bars: 150μm (A, M, O, P), 50 μm (C, E, G, I, K) and 350μm (R).

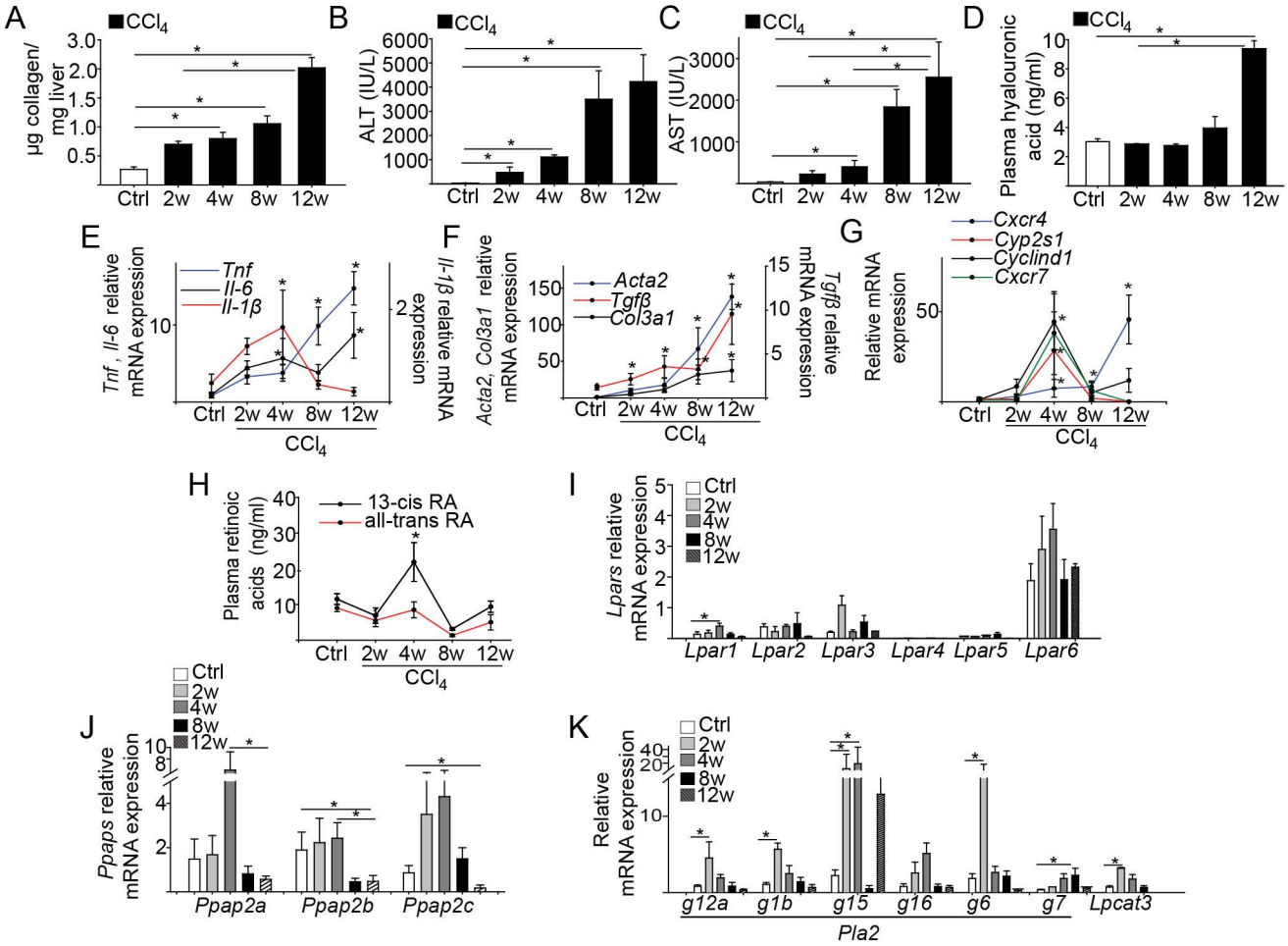

Fig. S2. CCl_4 hepatotoxicity stimulates liver damage, inflammation and fibrosis and alters the expression profile of *Lpars, Ppap2s* and *Pla2*. (A-C) Liver collagen deposition and liver damage, quantified by liver hydroxyproline levels and plasma transaminase (AST/ALT) levels respectively, in WT mice at the indicated time points post CCl_4 administration. (**D**) Hyaluronic acid plasma levels were quantified with a dedicated kit. **(E-G)** Q-RT-PCR analysis for the indicated mRNAs in liver extracts at the indicated time points. **(H)** HPLC-DAD determination of retinoic acid (RA) plasma levels at the indicated time points. **(I-K)** Q-RT-PCR analysis of relative mRNA expression of the indicated genes related to LPA signaling (*Lpars*) and catabolism (*Ppap2s*), as well as to LPC production (*Pla2*) in liver extracts 2-12w post CCl_4 administration. In all relative panels, Q-RT-PCR arbitrary values (standard curve method) were normalized to the expression levels of *Hprt* in the same samples. All values are mean +/- SEM. n=4-6. Unpaired, two sided Student's t-test for E-H *p<0.05 to control values (oil treated mice); ANOVA post hoc test for A-D, I-K.

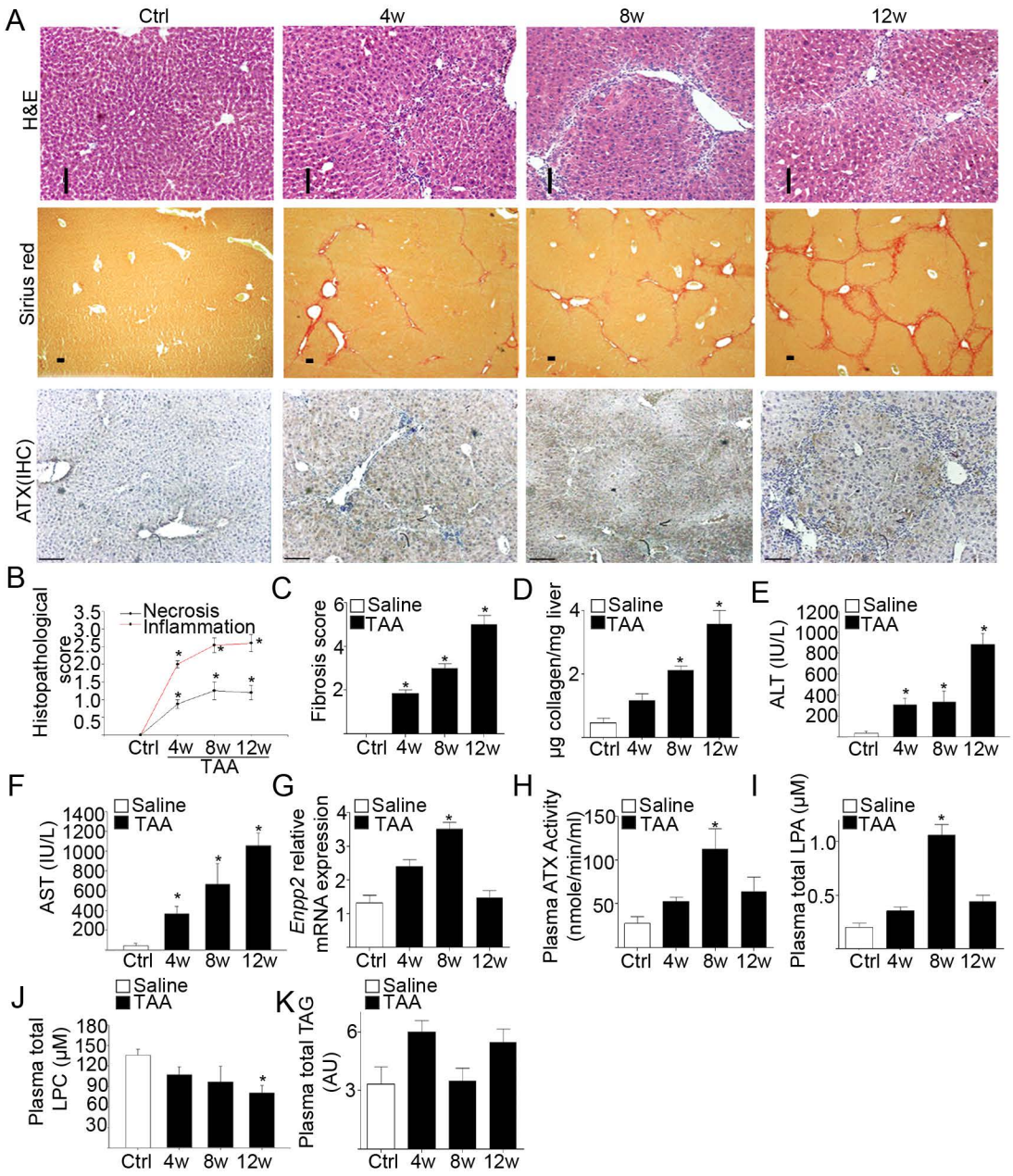

Fig. S3.Thiocetamide (TAA) hepatotoxicity stimulates autologous ATX expression and local LPA production. (**A**) Representative staining images of liver sections 4-12w post TAA administration in WT mice. (**B-C**) Semi-quantitative scoring of necrosis, inflammation and fibrosis. The Modified Ishaak scoring system was used for necroinflammation and fibrosis. Blind evaluations were performed from 2 independent reviewers and confirmed by 2 independent expert pathologists. (**D**) Liver collagen deposition was quantified by liver hydroxyproline levels. (**E-F**) Liver damage was assessed with plasma transaminase (AST, ALT) levels respectively. (**G**) *Enpp2* relative mRNA expression in liver extracts at the indicated time points. Q-RT-PCR arbitrary (ΔΔCt) values were normalized to the expression levels of *B2m* in the same samples and presented as fold change to control values. (**H**) Plasma ATX activity as measured with the TOOS assay. (**I-K**) Total levels of LPA/LPC/TAG species as determined with HPLC-ESI/MS/MS in plasma samples at the indicated time points. Values in graphs are mean +/- SEM; n=5-6; *p<0.05 to control (saline treated mice) values; unpaired, two sided Student's t-test. Scale bars: 50 µm.

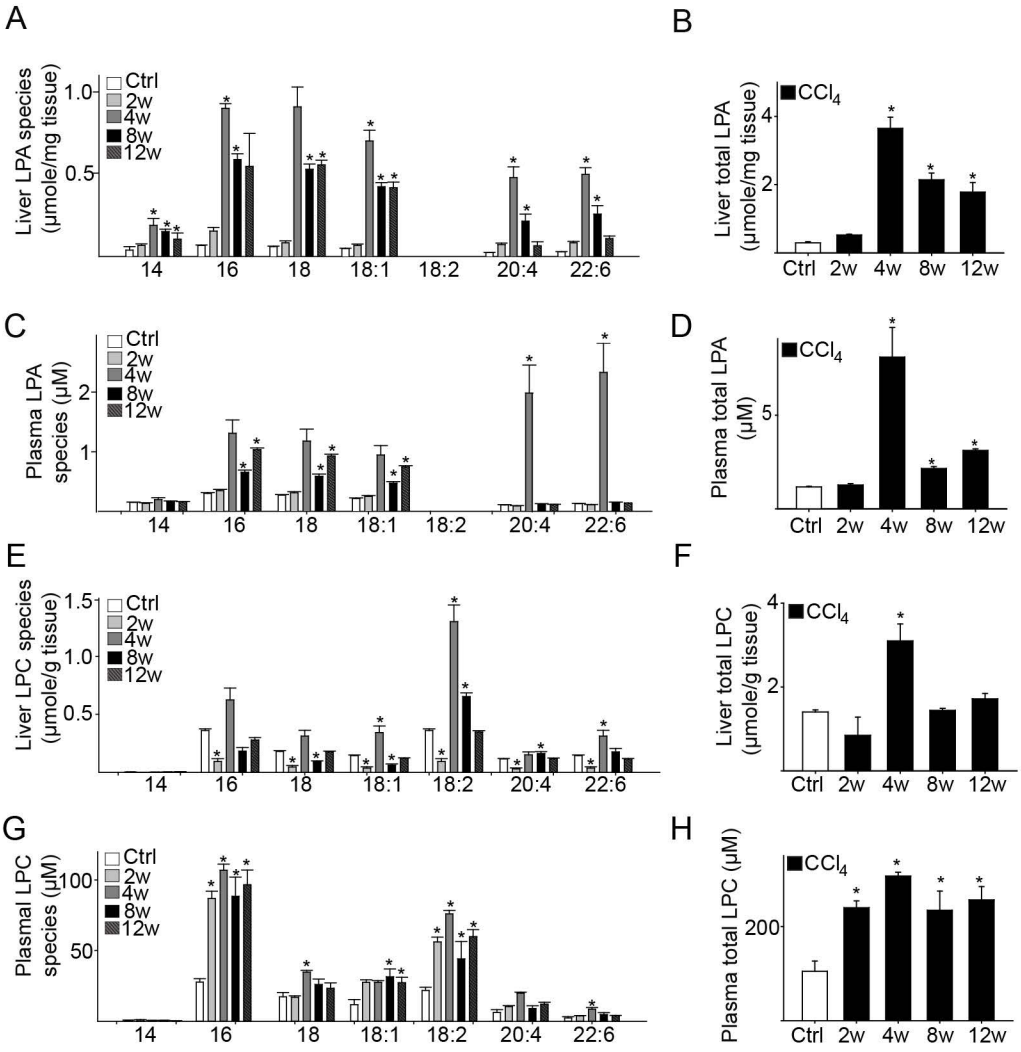

Fig. S4. CCl_4 hepatotoxicity distorts phospholipid homeostasis. (A-H) Total and individual LPA/LPC species levels in tissue/plasma respectively, 2-12w post CCl_4 administration in WT mice, as determined with HPLC-ESI/MS/MS. All values in graphs are mean +/- SEM; n=4-6; *p<0.05 to control (oil treated mice) values; unpaired, two sided Student's t-test.

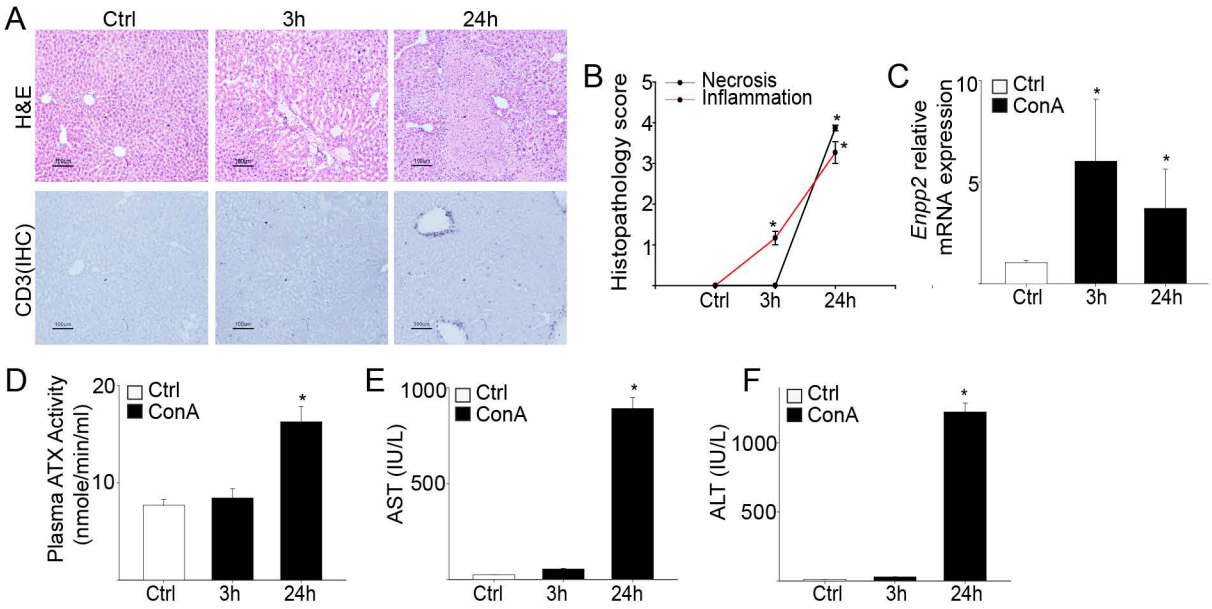

Fig. S5. Concavalin A (ConA) A-induced liver damage stimulates liver ATX expression. (**A**) Representative images from H&E and a-CD3 staining in liver sections post ConA administration. (**B**) Semi-quantitative scoring of necrosis and inflammation in the same liver sections. (**C**) *Enpp2* relative mRNA expression levels in the indicated liver extracts. Q-RT-PCR arbitrary (ΔΔCt) values were normalized to the expression levels of *b2m* in the same samples and presented as fold change to control values. (**D**) ATX activity, as determined with the TOOS assay, in the plasma of the respective mice. (**E-F**) Liver damage was quantified by plasma transaminase levels. Values in graphs are mean +/- SEM; n=5-6. *p<0.05 to control (saline treated mice) values; unpaired Student's t-test, two sided. Scale bars: 100μm.

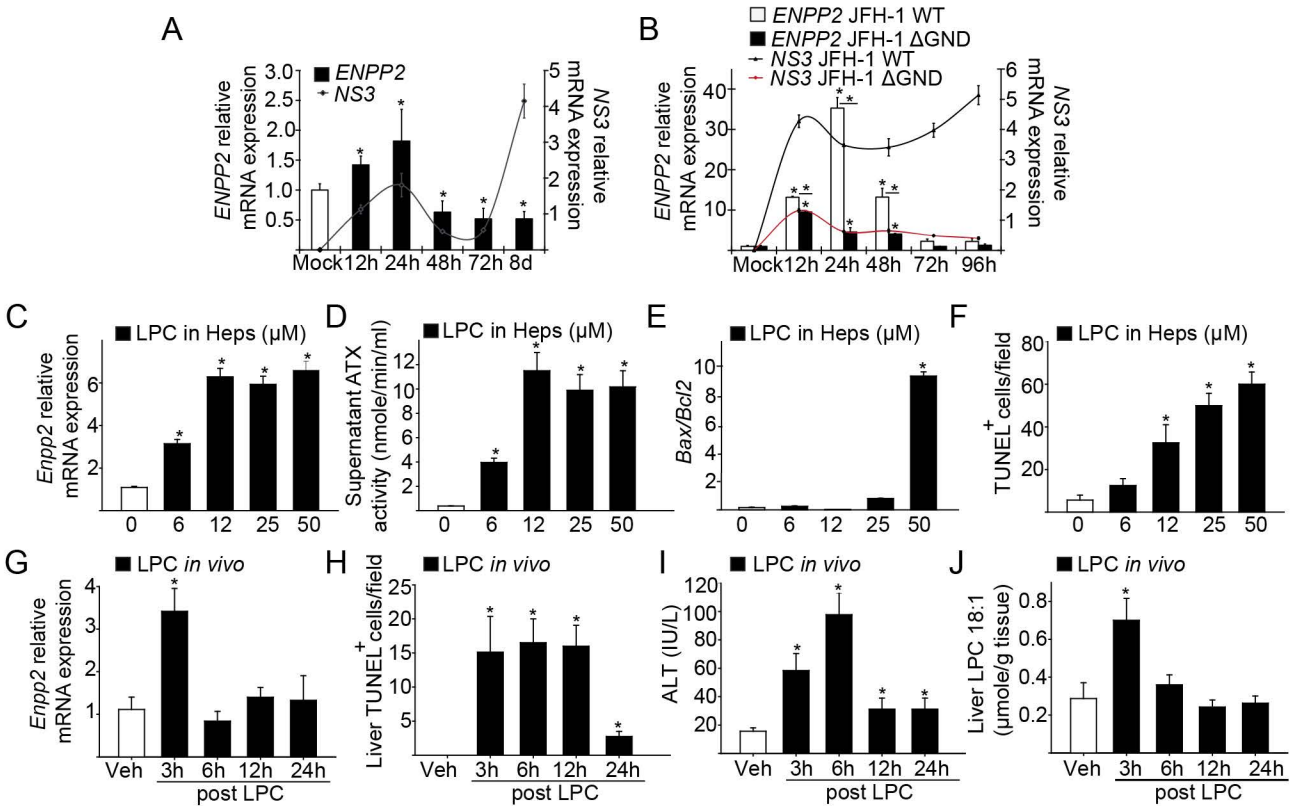

Fig. S6. HCV infection and exposure to LPC induce ATX expression. (**A-B**) Q-RT-PCR analysis for *ENPP2* and NS3 mRNA expression in HCV/JFH-1 infected Huh7.5 cells and pJFH-1 transfected HepG2 cells respectively. **(C)** Q-RT-PCR analysis for *Enpp2* mRNA relative expression in isolated Heps treated with different LPC (18:1) concentrations. **(D)** ATX activity measured with TOOS in the supernatant of the same cells, **(E)** Q-RT-PCR analysis of *Bax/Bcl2* **(F)** semi-quantitative scoring of apoptosis as determined by the number of TUNEL$^+$ cells in the same cells. **(G)** Q-RT-PCR analysis for *Enpp2* mRNA relative expression in liver extracts at the indicated hours post LPC (18:1, 60 mg/Kg) administration *in vivo*. **(H)** Semi-quantitative scoring of apoptosis in sections from the same livers described above. (**I**) Liver damage was assessed with transaminase levels in the plasma of the same mice and **(J)** Kinetic of LPC 18:1 in the liver measured with HPLC-ESI/MS/MS. In all relative panels, Q-RT-PCR arbitrary (ΔΔCt) values were normalized to the expression levels of *b2m* in the same samples and presented as fold change to control values. All values are mean +/- SEM; n=3-6;*p<0.05 to the respective control values (mock or vehicle) or indicated values; unpaired, two-sided, Student's t-test.

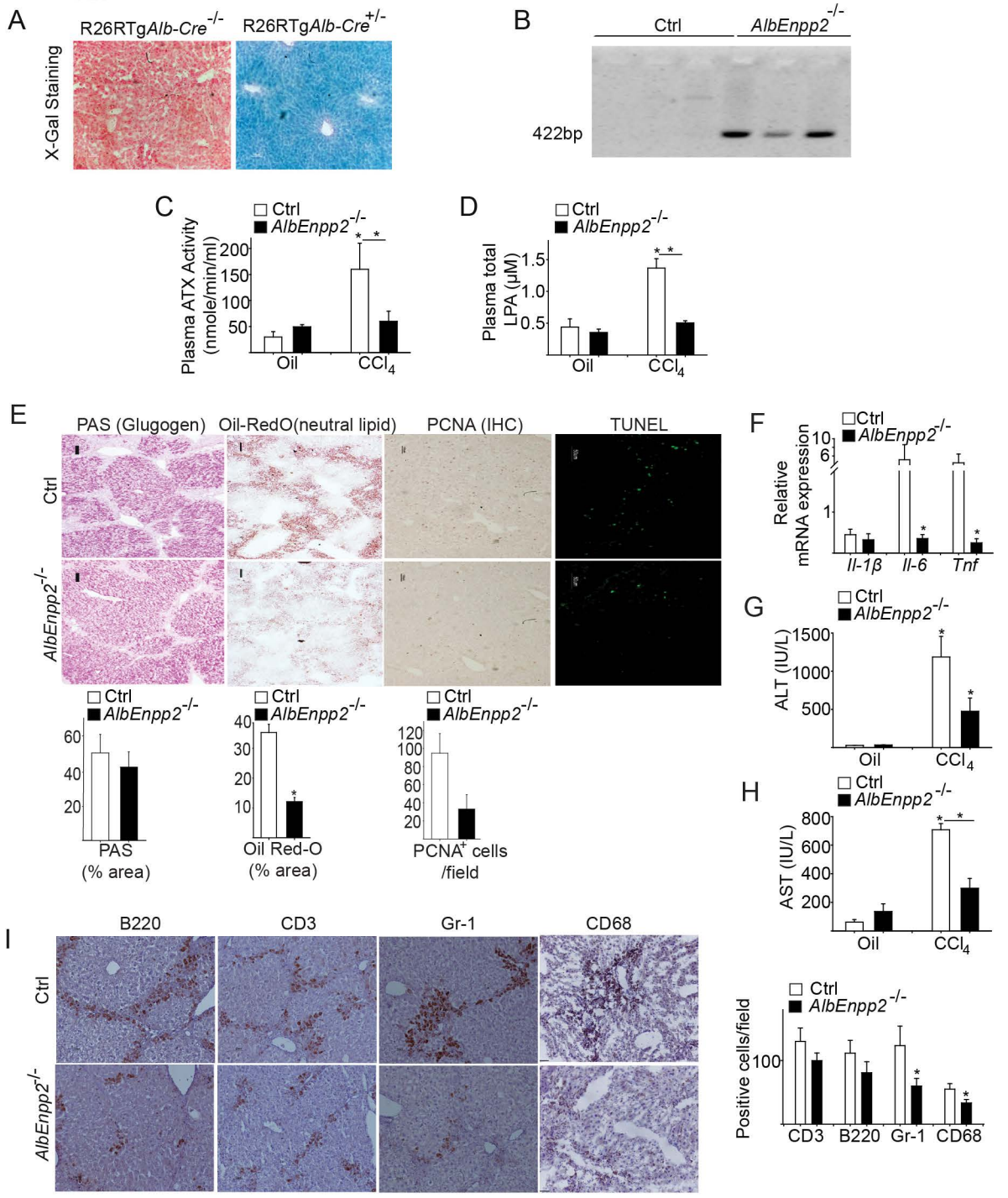

Fig. S7. Specific and accurate genetic deletion of ATX from hepatocytes in *AlbEnpp2*$^{-/-}$ mice modulates apoptosis, neutral lipid deposition, proliferation and liver inflammation. (**A**) Representative images from X-gal staining showing efficient activity of the albumin promoter driving cre recombinase expression in hepatocytes in the R26RTg*AlbCre* mice (**B**) Genomic PCR showing accurate recombination in *AlbEnpp2*$^{-/-}$ mice. (**C**) Plasma ATX activity measured with TOOS and **(D)** plasma LPA levels measured with HPLC-MS/MS at 4w post CCl_4 administration in *AlbEnpp2*$^{-/-}$ and control (Ctrl; Tg*Alb-Cre*) littermate mice**. (E)** Representative images from the indicated staining's in liver sections of the same mice treated with CCl_4 and their scoring. Scale bars: 100 μm with the exception of TUNEL 50 μm. **(F)** Q-RT-PCR analysis for inflammatory gene relative expression in liver extracts and **(G, H)** AST, ALT levels in the plasma of the same mice. **(I)** Representative IHC for the indicated cell specific markers and their scoring in liver sections from the indicated mouse strains 4w post CCl_4; Scale bars: 50 μm. Blind evaluation of all scoring was performed from 3 reviewers and confirmed by 2 independent expert pathologists. In all relative panels, Q-RT-PCR arbitrary (ΔΔCt) values were normalized to the expression levels of *b2m* in the same samples and presented as fold change to control values (oil treated mice). All values in graphs are mean +/- SEM; n=4-6; *p<0.05 to oil treated mice/indicated values (C, D, G, H) or to Ctrl:Tg*Alb-Cre* mice (E, F, I); unpaired Student's t-test, two sided.

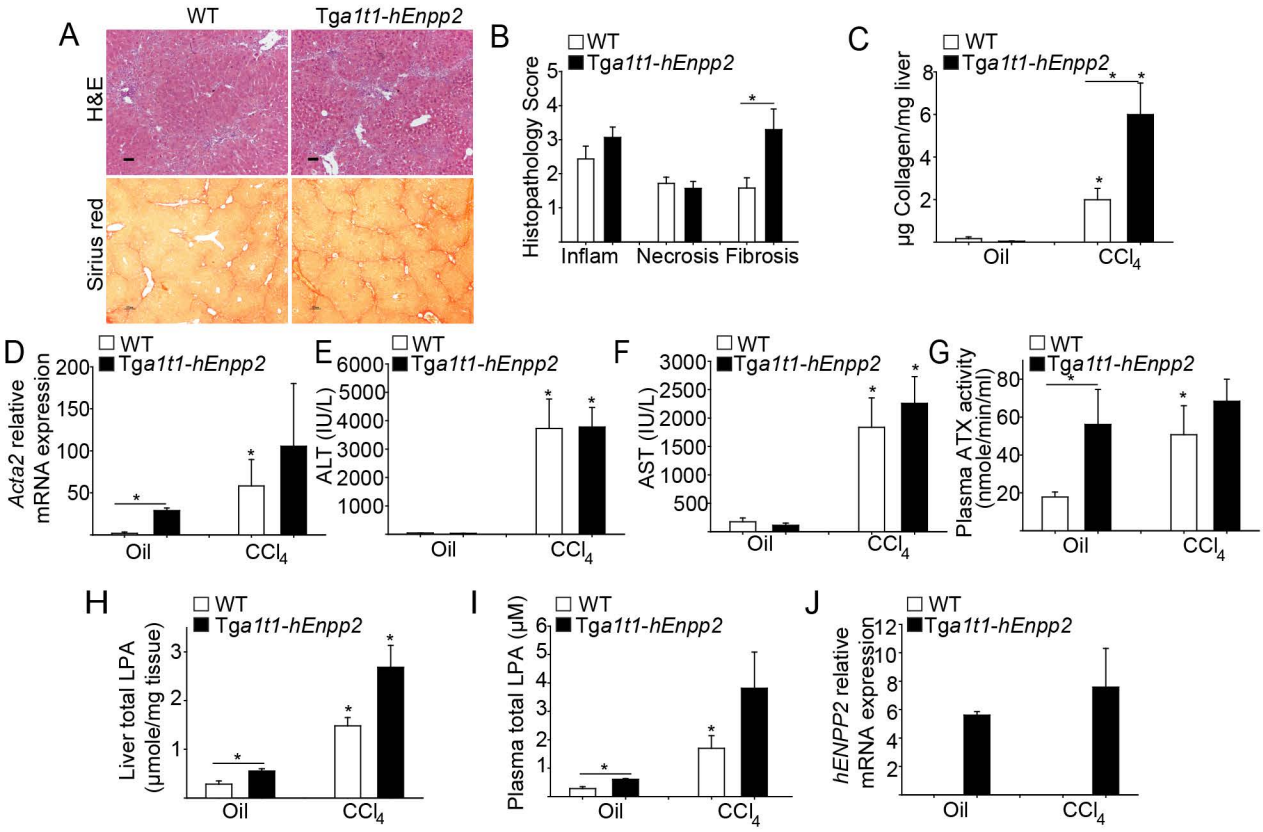

Fig. S8. Chronic hepatocyte-specific ATX transgenic overexpression exacerbates liver fibrosis. (**A**) Representative H&E and Sirius red staining (scale bars 25 and 50 µm respectively) in liver sections of the indicated mouse strains, 4w post CCl_4 administration. (**B**) Semi-quantitative scoring of necrosis, inflammation and fibrosis in the same liver sections. (**C**) Liver collagen deposition was quantified by liver hydroxyproline levels. (**D**) *Acta2/aSMA* relative mRNA expression, as determined with Q-RT-PCR. (**E-F**) Liver damage was quantified by plasma transaminase levels. (**G**) ATX plasma activity was determined with the TOOS assay. (**H-I**) Liver and plasma total LPA levels, as determined with HPLC-ESI/MS/MS. (**J**) Q-RT-PCR analysis of transgenic *hENPP2* expression in the same mice. In all relative panels, Q-RT-PCR arbitrary (ΔΔCt) values were normalized to the expression levels of *b2m* in the same samples and presented as fold change to control values. Blind evaluation of all histology scoring was performed from 2 reviewers and confirmed by 2 independent expert pathologists. WT: littermate controls of Tg*a1t1-hEnpp2* mice. All values are mean +/- SEM; n=5-12.*$p<0.05$ to the respective oil treated controls or indicated values; unpaired, two-sided Student's t-test, or Mann-Whitney for non-normal distributions.

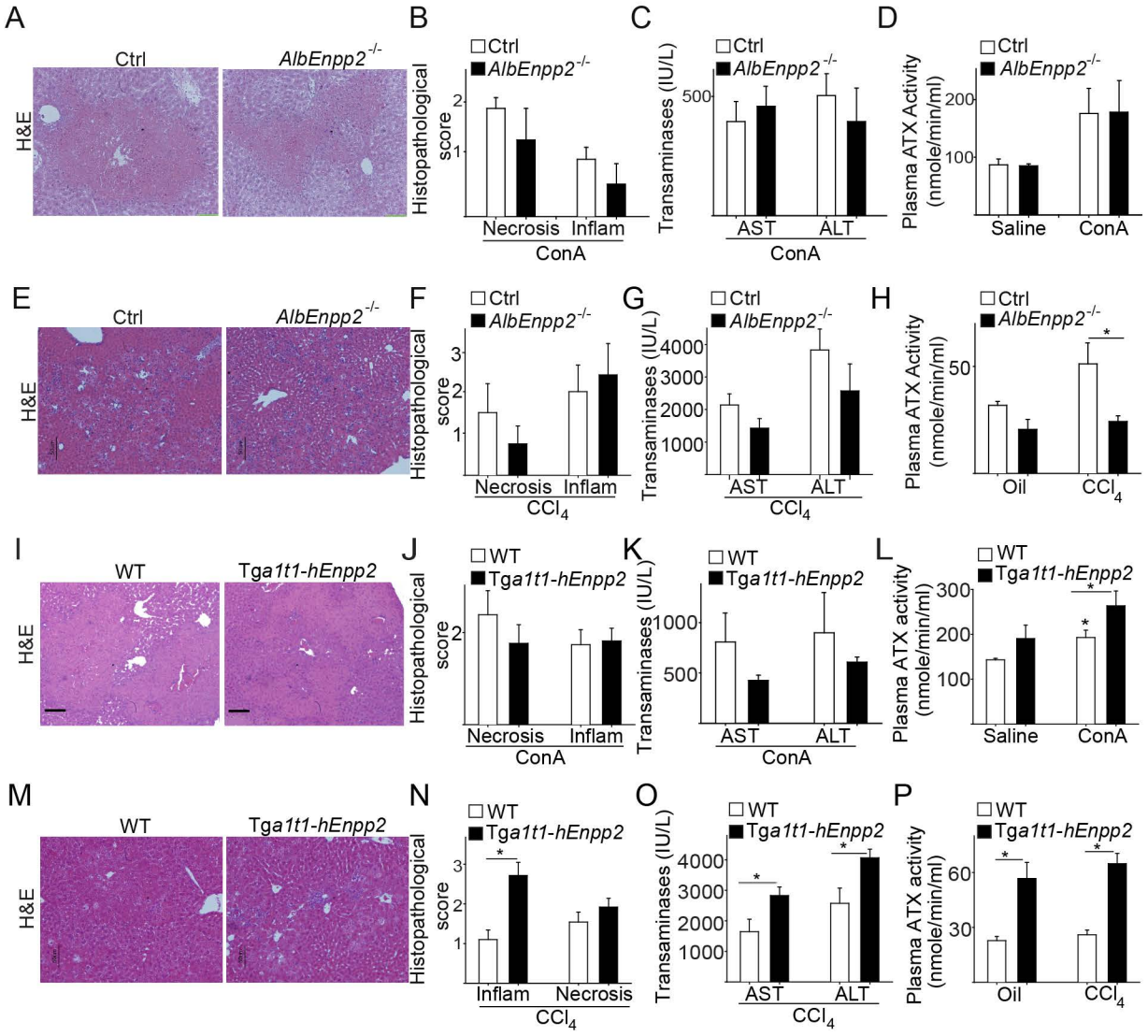

Fig. S9. Hepatocyte-specific genetic deletion or transgenic overexpression of ATX has minimal effects in acute liver damage. (**A, E, I, M**) representative H&E staining and (**B, F, J, N**) semi-quantitative scoring of necrosis and inflammation in liver sections of the indicated mouse strains 24h post ConA or CCl_4 administration respectively; blind evaluation of all histology scoring was performed from 3 reviewers and confirmed by 2 independent expert pathologists. (**C, G, K, O**) Transaminase and (**D, H, L, P**) ATX activity levels in the plasmas of the same mice. Ctrl: *Enpp2*$^{n/n}$ mice. WT: littermate controls of Tg*a1t1-hEnpp2* mice. All values in graphs are mean +/- SEM; n=6-8; *p<0.05 to oil/saline treated littermate controls or indicated values; unpaired, two sided Student's t-test. Scale bars: 50 μm.

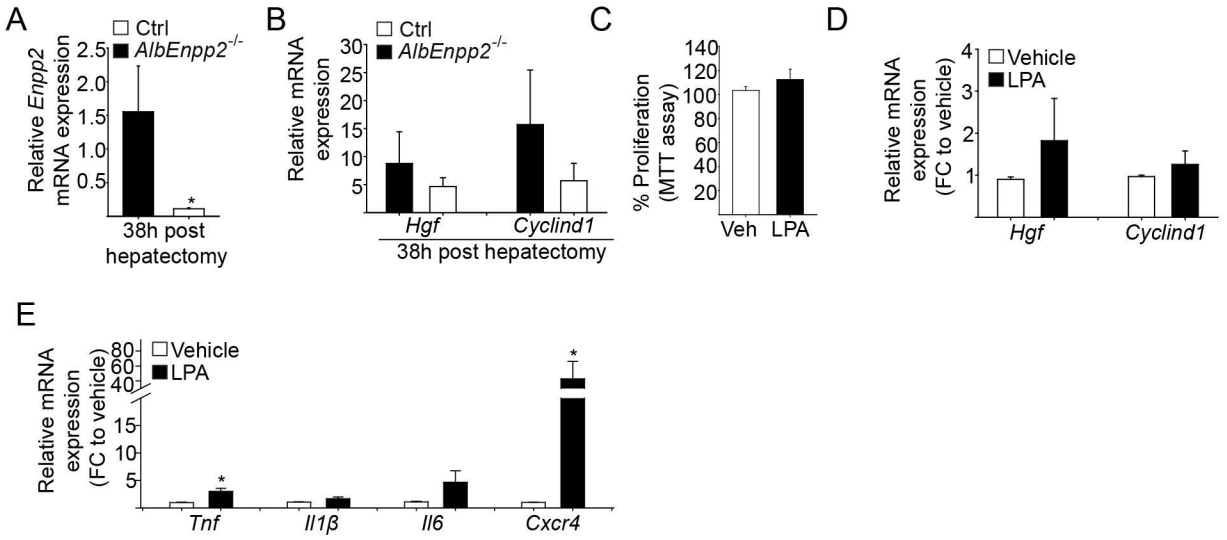

Fig. S10. Effects of LPA on Heps. (**A B**) Partial (2/3) hepatectomy in the presence (Ctrl: *Enpp2*$^{n/n}$ mice) or absence of ATX from Heps (*AlbEnpp2*$^{-/-}$ mice) and the measurement of *Enpp2, Hgf and Cyclind1* gene expression with Q-RT-PCR 38 h post hepatectomy. (**C**) Proliferation assay with MTT, (**D**) Growth/proliferation related genes mRNA expression and (**E**) Inflammatory genes mRNA expression, as measured with Q-RT-PCR in cultured Heps isolated from WT mice and treated with 10μM LPA 18:1 for 24 h. Q-RT-PCR arbitrary (ΔΔCt) values were normalized to the expression levels of *hprt* in the same samples and presented as fold change to vehicle treated cells (D, E). All values in graphs are mean +/- SEM; n=3-4; *p<0.05 to littermate controls *Enpp2*$^{n/n}$ mice or to vehicle treated Heps; unpaired, two sided Student's t-test.

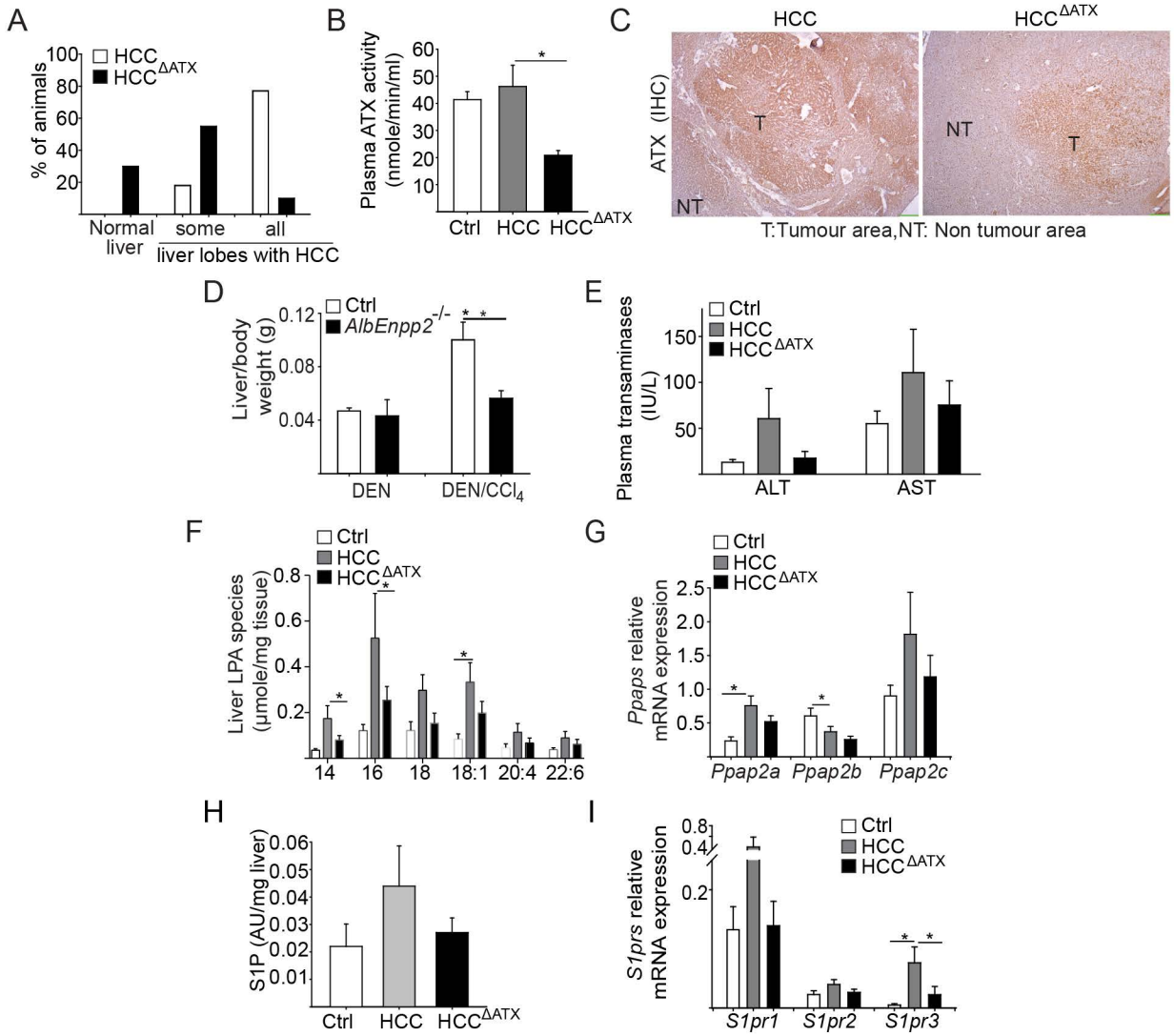

Fig. S11. Genetic deletion of ATX from hepatocytes diminish HCC incidence and attenuates LPA. (**A**) Cancer incidence of the indicate mice treated with DEN/CCl_4 in the presence (HCC) or in the absence of ATX from hepatocytes ($HCC^{\Delta ATX}$). (**B**) Plasma ATX activity in the same mice was quantified with the TOOS assay. (**C**) Representative ATX staining of liver sections of the indicated mouse strains post DEN/CCl_4 administration; Scale bar: 300 µm. (**D**) Relative liver weight, Ctrl: *Enpp2*$^{n/n}$ mice and (**E**) plasma transaminase levels from the indicated mouse strains post DEN/CCl_4 administration and saline/oil (Ctrl). (**F**) LPA species levels in the livers of the indicated mouse strains and treatments, as determined with HPLC-ESI/MS/MS. (**G**) Q-RT-PCR analysis of *Ppap2s* relative mRNA expression. Q-RT-PCR arbitrary values (standard curve method) were normalized to the expression levels of *Hprt* in the same samples. (**H**) Total S1P (species C16, C18) levels in the livers of the indicated mouse strains and treatments, as determined with HPLC-ESI/MS/MS. (**I**) Q-RT-PCR analysis of *S1prs* relative mRNA expression. Q-RT-PCR arbitrary values (standard curve method) were normalized to the expression levels of *Hprt* in the same samples. All values in graphs are mean +/- SEM; n=7-14; *p<0.05 to respective control (Ctrl: saline/oil treated mice) or indicated values; unpaired Student's t-test, two-sided or Mann-Whitney for non-normal distributions.

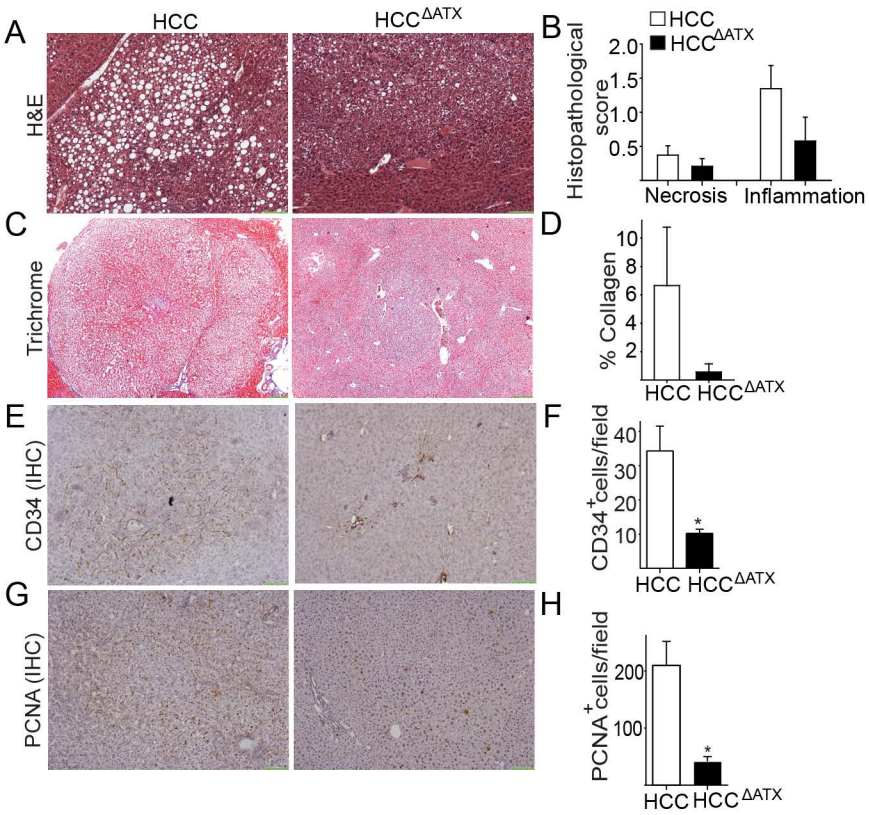

Fig. S12. Genetic deletion of ATX in DEN/CCl_4-treated mice attenuates proliferation and angiogenesis. (**A, C, E, G**) Representative staining with the indicated stains of liver sections (tumour area) from the indicated mouse strains post DEN/CCl_4 administration in the presence (HCC) or in the absence of hepatocyte ATX expression ($HCC^{\Delta ATX}$). Scale bars: 150 µm (H&E), 300 µm (Trichrome staining), 60 µm (CD34, PCNA). (**B**) Semi-quantitative scoring of necrosis and inflammation. (**D**) Liver collagen deposition in the livers of the same mice was estimated semi-quantitatively by trichrome staining and presented as % collagen deposition per optic field. (**F, H**) Semi-quantitative scoring of angiogenesis ($CD34^+$ cells) and proliferation ($PCNA^+$ cells). Blind evaluation of all histology scoring was performed from 2 reviewers and confirmed by 2 independent expert pathologists. All values are mean +/- SEM. n=7-12. *$p<0.05$ to respective littermate control (HCC); unpaired, two-sided Student's t-test.

Supporting Table S1. Expression profiles of the ATX/LPA axis genes and PLA2s in public microarray datasets. Data mining in all CLD and HCC patient microarray datasets publically available at NCBI/GEO, using the embedded tool GEO2R. Values shown are only statistical significant ($p<0.05$) fold changes over controls identified for each dataset – patient cohort. n*: patients/controls; Datasets and microarray platforms are hyperlinked. HCV: chronic hepatitis C; HBV: chronic hepatitis B; NASH: non-alcoholic steatohepatitis; NAFLD: nonalcoholic fatty liver disease; ALD: Alcoholic liver disease; HCC: Hepatocellular Carcinoma; Alcohol: alcohol abuse related Hepatopathy

A. mRNA expression profile of ATX-LPA axis genes in Hepatitis patients liver tissue

Disease	Dataset	Platform	n*	ATX	LPAR1	LPAR2	LPAR3	LPAR4	LPAR5	LPAR6	PPAP2A	PPAP2B	PPAP2C	Ref
HCV	GSE33650	GPL14877	32/40	-	-	1.16	-	1.27	-	-1.62	-	-1.31	-	[1]
Cirrhosis	GSE6764	GPL570	10/10	4.1	-	1.21	-	-	2.01	1.75	1.27	-	2.58	[2]
Cirrhosis	GSE14323	GPL571	41/19	6.32	1.65	1.12	-1.27	-	-	3.03	1.3	1.27	1.75	[3]
Cirrhosis	GSE25097	GPL10687	40/6	2.64	2.27	2.43	1.88	-	4.26	3.53	-	-2.56	3.01	[4]
Cirrhosis	GSE36411	GPL570	21/21	2.13	-	-	-	-	-	1.18	-	-	-	n.a.
ALD	GSE28619	GPL570	15/7	4.5	1.16	-	-	-	-	1.85	1.98	-2.37	2.58	[5]
NASH	GSE17470	GPL2895	6/4	-	-	-	-	-	-	5.43	-	4.04	-	[6]
NASH	GSE24807	GPL2895	12/5	2.66	2.08	-	-	-	-	11.39	-	4.94	-	[7]
NASH	GSE63067	GPL570	9/7	1.93	-	-	-	-	-	-	-	1.91	-	[8]
NASH	GSE33814	GPL6884	31/13	1.95	1.38	1.29	-	1.05	-	1.27	-1.21	-1.52	1.15	[9]
NAFLD	GSE48452	GPL11532	32/14	-	-	-	-	-	-	-	-	-	-	[10]
NAFLD	GSE49541	GPL570	32/40	2.37	1.21	-	-	-	-	-	-	-	-	[11]

B. mRNA expression profile of ATX-LPA axis genes in HCC patients liver tissue

Disease	Dataset	Platform	n*	ATX	LPAR1	LPAR2	LPAR3	LPAR4	LPAR5	LPAR6	PPA2PA	PPAP2B	PPAP2C	Ref
Early HCC vs wt	GSE6764	GPL570	18/10	-	-	-	-	-	-1.09	-	1.59	-2.24	-	[2]
Adv. HCC vs wt	GSE6764	GPL570	17/10	-	-1.18		-1.22	-1.18	-1.12	-1.07	1.85	-3.34	-	[2]
HCC vs wt	GSE14323	GPL571	38/19	4.69	1.40	1.15	-	1.07	-	2.55	1.29	-1.77	1.24	[3]
Young HCC vs wt	GSE45267	GPL570	16/39	3.68	-1.26	1.34	1.46	-	-1.19	-	-1.47	-3.35	3.43	n.a.
Senior HCC vs wt	GSE45267	GPL570	32/39	-	-1.34	-	-1.18	-	-1.14	-1.40	1.45	-2.72	-	n.a.
HCC vs wt	GSE62232	GPL570	17/10	-	-1.41	-	-1.36	-1.14	-	-	1.67	-2.26	-	n.a.
Undiff HCC vs wt	GSE36411	GPL10558	21/21	3.90	-	-	-	-	-	-	-1.19	-2.06	-	n.a.
diff. HCC vs wt	GSE36411	GPL10558	21/21	2.86	-	-	-	-	-	-	1.54	-2.09	-1.01	n.a.
HBV HCC vs wt	GSE50579	GPL14550	8/10	6.19	-	1.87	-	-	-	-	1.79	-	-	[12]
HBV HCC vs wt	GSE62232	GPL570	16/10	3.51	-1.46	-	-1.39	-1.11	-1.22	-	1.46	-2.86	2.33	n.a.
HCV HCC vs wt	GSE50579	GPL14550	8/10	4.59	-	1.67	-	-	-	-	1.75	-1.89	-	[12]
HCV HCC vs wt	GSE62232	GPL570	15/10	-	-1.55	-	-1.25	-1.13	-	-	1.65	-2.50	-	n.a.
Alc. HCC vs wt	GSE50579	GPL14550	10/10	3.71	-	-	-	-	-	-	2.75	-1.78	-	[12]
Alc. HCC vs wt	GSE62232	GPL570	33/10	-	-1.48	-	-1.39	-1.09	-	-	1.55	-2.41	-	n.a.

C. mRNA expression profile of PLA2 genes in Hepatitis patients liver tissue

Disease	Dataset	Platform	n*	g1B	g2A	g2C	g2D	g2E	g2F	g3	g4A	g4B	g4C	g4D	g4E	g4F	g5	g6	g7	g10	g12A	g12B	g15	g16	Ref
HCV	GSE33650	GPL14877	32/40	-	-	-	-	-	-	-	1.27	-	-	-	-	1.27	-	-	-	-	-1.53	-	-	-	[1]
Cirrhosis	GSE6764	GPL570	10/10	-	-	-	-	-	-	-	1.82	-	**2.35**	-	-	-	**2.64**	-	-	-	-1.29	-1.33	-	-1.31	[2]
Cirrhosis	GSE14323	GPL571	41/19	-	-	-	-1.21	-1.29	-1.13	-1.31	1.84	-	**2.69**	-	-	-	**2.07**	-1.19	2.97	-1.33	-	-	-	-1.42	[3]
Cirrhosis	GSE25097	GPL10687	40/6	-	-	-	**2.14**	-1.16	-	-	**3.25**	-	**2.81**	-	-	-	1.89	-	**11.08**	-	**-2.03**	-	1.89	-	[4]
Cirrhosis	GSE36411	GPL570	21/21	-	-	-	-1.06	-	-	-	-	-	1.65	1.08	-	-	-	-	1.29	-	-	-	-	-	n.a.
ALD	GSE28619	GPL570	15/7	-	-	-	-	-	-	-	1.54	-	**2.55**	-	-	-	-	-	**3.68**	-	-1.58	1.28	-	-1.60	[5]
NASH	GSE17470	GPL2895	6/4	-	-	-	-	-	-	1.72	-	-	-	-	-	-	**3.53**	-	**3.41**	-	-	-	**-4.03**	**-2.31**	[6]
NASH	GSE24807	GPL2895	12/5	-	-	-	**-2.08**	-	-	-	-	-	**2.35**	-	-	-	**6.32**	-	**4.56**	-	1.65	**2.00**	**-2.31**	-	[7]
NASH	GSE63067	GPL570	9/7	-	-	-	-	-	-	-	-	-	-	-	-	-	-	-	-	-	-	-	-	-	[8]
NASH	GSE33814	GPL6884	31/13	-1.16	-	-	-	-	-	-	-	-	1.68	-	-	-	-	-	-	1.08	-	-	-	-1.33	[9]
NAFLD	GSE48452	GPL11532	32/14	-	-	-1.14	-	-	-	-	-	-	-	-	-	-	-	-	-	-	-	-	-	-1.22	[10]
NAFLD	GSE49541	GPL570	32/40	-	-	-	-	-	-	-	1.26	-	1.23	-	-	-	-	-	-	-	-1.27	-	-	-1.34	[11]

D. mRNA expression profile of PLA2 genes in HCC patients liver tissue

Disease	Dataset	Platform	n*	g1B	g2A	g2C	g2D	g2E	g2F	g3	g4A	g4B	g4C	g4D	g4E	g4F	g5	g6	g7	g10	g12A	g12B	g15	g16	Ref
Early.HCC vs NT	GSE6764	GPL570	18/10	-	-	-	-	-	-	-1.06	-	-	**3.14**	-	-	-	-	1.48	-	-	-1.54	-	-1.36	**-2.58**	[2]
Adv.HCC vs NT	GSE6764	GPL570	17/10	-	-	-	-	-1.10	-	-	-	-	**2.22**	-1.06	-	-	-	-	**2.25**	-	-1.64	-1.64	-1.58	**-3.25**	[2]
HCC vs NT	GSE14323	GPL571	38/19	-	-	-	-	-	-	-	1.35	-	**2.33**	-	-	-	-	-1.16	**2.43**	-	-1.73	-	-	**-2.06**	[3]
youngHCC vs NT	GSE45267	GPL570	16/39	-	**-11.31**	-	-	-	-	-1.20	-1.28	-	1.59	-1.14	-	-	-1.93	1.57	-	-	-1.77	-1.49	-	-1.93	n.a.
seniorHCC vs NT	GSE45267	GPL570	32/39	1.64	-	-	-1.23	-1.15	-	-1.21	-1.22	-	1.40	-1.09	-	-1.33	-1.42	-	-	-1.13	-1.42	-	-	-1.47	n.a.
noEtiology.HCC vs NT	GSE62232	GPL570	17/10	-	-	-	-	-1.14	-	-1.30	-	1.17	**2.93**	-1.16	-	-	-1.24	-	1.39	-	-1.34	-	-	-1.81	n.a.
undiff.HCC vs NT	GSE36411	GPL10558	21/21	1.74	-1.97	-1.07	-	-	-	1.13	-	-	1.61	1.12	-	-	-1.27	-	2.35	-	-1.17	-	-	**-2.43**	n.a.
diff.HCC vs NT	GSE36411	GPL10558	21/21	1.34	-	-	-	-	-	1.09	-	-	1.95	1.12	-	-	-	-	1.42	-	-1.08	-	-1.30	**-2.23**	n.a.
HBV.HCC vs NT	GSE50579	GPL14550	8/10	-	-	-	-	-	-	-	-	-	**3.36**	-	-	-	-	-	**3.76**	-	-1.82	-	-1.62	-	[12]
HBV.HCC vs NT	GSE62232	GPL570	16/10	-	-	-	-	-1.14	-	-1.32	-	-	**3.46**	-1.21	-	-1.22	-1.30	-	2.75	-	-1.62	-	-1.23	**-2.38**	n.a.
HCV.HCC vs NT	GSE50579	GPL14550	8/10	-	-	-	-	-	-	-	-	-	2.64	-	-	-	-	-	**4.96**	-	-1.74	-	-	**-2.95**	[12]
HCV.HCC vs NT	GSE62232	GPL570	15/10	-	-	-	-	-1.21	-	-1.36	-	-	**2.77**	-1.17	-	-1.25	-1.51	1.20	1.61	-1.16	-1.53	-	-	-1.89	n.a.
Alcohol .HCC vs NT	GSE50579	GPL14550	10/10	-	-	-	-	-	-	-	-	-	**3.56**	-	2.17	-	-	-	**4.17**	-	-1.47	-	-	**-2.33**	[12]
Alcohol .HCC vs NT	GSE62232	GPL570	33/10	-	-	-	-	-1.16	-	-1.31	-	-	**2.81**	-1.18	-	-1.16	-1.46	-	-	-	-1.34	-	-	-1.63	[2]

References

1. Munshaw, S., et al., *Laser captured hepatocytes show association of butyrylcholinesterase gene loss and fibrosis progression in hepatitis C-infected drug users.* Hepatology, 2012. **56**(2): p. 544-54.
2. Wurmbach, E., et al., *Genome-wide molecular profiles of HCV-induced dysplasia and hepatocellular carcinoma.* Hepatology, 2007. **45**(4): p. 938-47.
3. Mas, V.R., et al., *Genes involved in viral carcinogenesis and tumor initiation in hepatitis C virus-induced hepatocellular carcinoma.* Mol Med, 2009. **15**(3-4): p. 85-94.
4. Tung, E.K., et al., *Clinicopathological and prognostic significance of serum and tissue Dickkopf-1 levels in human hepatocellular carcinoma.* Liver Int, 2011. **31**(10): p. 1494-504.
5. Affo, S., et al., *Transcriptome analysis identifies TNF superfamily receptors as potential therapeutic targets in alcoholic hepatitis.* Gut, 2013. **62**(3): p. 452-60.
6. Baker, S.S., et al., *Role of alcohol metabolism in non-alcoholic steatohepatitis.* PLoS One, 2010. **5**(3): p. e9570.
7. Liu, W., et al., *Upregulation of hemoglobin expression by oxidative stress in hepatocytes and its implication in nonalcoholic steatohepatitis.* PLoS One, 2011. **6**(9): p. e24363.
8. Frades, I., et al., *Integrative genomic signatures of hepatocellular carcinoma derived from nonalcoholic Fatty liver disease.* PLoS One, 2015. **10**(5): p. e0124544.
9. Starmann, J., et al., *Gene expression profiling unravels cancer-related hepatic molecular signatures in steatohepatitis but not in steatosis.* PLoS One, 2012. **7**(10): p. e46584.
10. Ahrens, M., et al., *DNA methylation analysis in nonalcoholic fatty liver disease suggests distinct disease-specific and remodeling signatures after bariatric surgery.* Cell Metab, 2013. **18**(2): p. 296-302.
11. Murphy, S.K., et al., *Relationship between methylome and transcriptome in patients with nonalcoholic fatty liver disease.* Gastroenterology, 2013. **145**(5): p. 1076-87.
12. Neumann, O., et al., *Methylome analysis and integrative profiling of human HCCs identify novel protumorigenic factors.* Hepatology, 2012. **56**(5): p. 1817-27.

Supporting Table S2. Patients' characteristics, ATX levels, laboratory tests and their correlations

	Controls		Patients		Viral		NASH		ALD	
	M	**F**	**M**	**F**	**M**	**F**	**M**	**F**	**M**	**F**
N, (%)	8 (40%)	12 (60%)	29 (48%)	30 (52%)	14 (38%)	21 (62%)	5 (42%)	7 (58%)	10 (83%)	2 (17%)
Age (years)	59 (29-66)	49 (30-81)	55 (21-84)	57 (26-82)	45 (21-76)	57 (26-82)	47 (26-63)	57 (51-74)	62 (38-84)	58 (50-65)
BMI (Kg/m^2)	26 (24-30)	25 (23-32)	28 (21-36)	26 (18-45)	26 (21-34)	25 (18-36)	30* (24-36)	33* (27-45)	28 (23-33)	22 (20-23)
Cirrhosis (yes/no)	-	-	12/17	5/25	2/12	3/18	1/4	0/7	10/0	2/0
Therapy (yes/no)	-	-	6/23	8/22	6/8	8/13	0/5	0/7	0/10	0/2
Viral Active (yes/no)	-	-	5/24	7/23	5/9	7/14	-	-	-	-
Statins (yes/no)					2/12	1/20	1/4	5/2		
	Laboratory tests									
Autotaxin (ATX) ng/ml	129 (18-195)	183 (91-347)	194* (128-3500)	217* (43-1299)	189* (128-3500)	166 (43-1299)	159* (124-688)	255* (141-1140)	301* (135-597)	196 (172-221)
Alanine transaminase (ALT) (IU/L)	18 (11-30)	20 (11-27)	32* (11-102)	36* (8-103)	44* (17-102)	38* (13-103)	41* (25-53)	27* (14-103)	23 (11-56)	22 (8-35)
Aspartate transaminase (AST) (IU/L)	20 (15-26)	19 (12-59)	23* (11-101)	31* (13-83)	23* (11-101)	31* (13-83)	24* (21-54)	31 (20-56)	20 (15-37)	26 (21-30)
Platelets (PLT) (x10^9/L)	216 (129-335)	233 (145-283)	199 (120-607)	211 (100-555)	200 (122-607)	225 (100-555)	221 (185-274)	198 (139-262)	174 (120-321)	143 (140-146)
γ-glutamyl transferase (γGT) (IU/L)	18 (12-29)	13 (6-29)	43* (10-192)	25* (9-115)	32* (10-192)	24 (10-76)	43* (33-54)	19 (9-68)	49* (27-103)	72 (28-115)
Alkaline Phosphatase (ALP) (IU/L)	57 (38-65)	63 (42-82)	74* (45-363)	79* (46-182)	85* (45-363)	89* (46-182)	102* (63-180)	117* (91-486)	118* (72-305)	241* (133-49)
Albumin (ALB) (g/dL)	4.4 (4-4.7)	4.3 (4-4.6)	4.3 (2.5-5.6)	4.2 (1-4.8)	4.4 (3.2-5)	4.2 (1-4.7)	4.5 (4.1-5.6)	4.3 (3.8-4.8)	4.2 (2.5-4.9)	3.6 (3.2-4.2)
Total protein-Albumin (TP-Alb)	3 (2.5-3.3)	2.9 (2.4-3.8)	3.2* (2.5-5.9)	3.5* (2.6-12)	3* (2.5-5.9)	3.5* (2.6-12)	2.8 (2.5-3.8)	3.2* (2.6-4.6)	3.5* (2.5-4.4)	3.9 (3.8-4)
Total Bilirubin (TBIL) (mg/dL)	0.1 (0.09-0.3)	0.1 (0.04-0.5)	0.2* (0.06-0.9)	0.2* (0.09-0.7)	0.3* (0.06-0.9)	0.2* (0.09-0.7)	0.2 (0.1-0.3)	0.2 (0.1-0.4)	0.2* (0.09-0.9)	0.2 (0.1-0.2)
Cholesterol (Chol) (mg/dL)	180 (108-268)	212 (163-270)	172 (77-392)	183 (66-251)	169 (77-392)	180 (102-251)	185 (101-240)	188 (66-209)	173 (153-311)	216 (185-248)

Triglycerides (TG) (mg/dL)	81 (63-192)	76 (55-111)	132 (11-304)	87 (42-322)	177* (11-224)	84 (57-322)	178* (58-276)	142 (42-205)	100 (66-304)	144 (84-203)
Creatinine (CR) (mg/dL)	1 (0.8-1.2)	0.8 (0.6-1)	1 (0.8-1.6)	0.8 (0.4-1.4)	0.9 (0.8-1.4)	0.8 (0.4-1.4)	1.3 (1.1-1.6)	0.9 (0.7-1.1)	1 (0.9-1.5)	0.9 (0.7-1)
Alpha-Fetoprotein (aFP) (ng/ml)			2.4 (0.7-7.7)	3.4* (0.6-40)	2.4 (0.7-4.7)	1.9* (0.6-40)	1.1 (0.8-1.2)	1.9 (3.4-10)	3 (2.2-7.7)	6.6 (5-7)
Superoxide Dismutase (SOD) (kU/grHb)	42 (9-54)	44 (19-60)	47 (2-116)	39 (7-85)	35 (2-63)	39 (12-85)	54* (50-116)	55 (8-62)	44 (7-59)	35 (18-52)
Glutathione (GSH) (µM)	1515 (442-3020)	1077 (276-636)	482* (1-1356)	485* (47-2076)	409* (1-1356)	774 (47-2076)	678 (447-1266)	296* (65-1243)	374* (5-903)	585 (469-500)
%GSSG/Total GSH	4 (0.5-16)	6.8 (0.3-14)	18* (0.2-184)	11* (0.1-75)	20* (0.2-184)	6 (0.1-47)	32* (10-44)	27* (2.5-75)	0.3* (4-98)	2.3 (2.7-3.2)

*Median values are shown; *p<0.05 denotes statistical significance to control sex-matched group; Mann Whitney test.*

Supporting Table S3. Correlations of the levels of ATX and laboratory parameters

Parameter	r	p
Platelets (PLT)	-0,2	0,06
Creatinine (CR)	-0,03	0,7
Albumin (ALB)	-0,2	0,03
Total protein-Albumin (TP-Alb)	0,3	0,003
Aspartate transaminase (AST)	0,4	<0,0001
Alanine transaminase (ALT)	0,4	0,002
Cholesterol (Chol)	0,5	0,0002
Alkaline Phosphatase (ALP)	0,6	<0,0001
γ-glutamyl transferase (γGT)	0,5	<0,0001
Total Bilirubin (TBIL)	0,6	<0,0001
Triglycerides (TAG)	0,3	0,02
Alpha-Fetoprotein (aFP)	0,3	0,05
Superoxide Dismutase (SOD)	-0,2	0,08
Glutathione (GSH)	-0,4	0,008
%GSSG/Total GSH	0,6	<0,0001

Supporting Table S4. Gene set enrichment analysis of differentially expressed genes upon the genetic deletion of ATX in hepatocytes and HCC development.
(*AlbEnpp2*$^{-/-}$ mice vs littermate control mice 30/14w post DEN/CCl_4 treatment respectively)

Category	Term	Count	%	p Value	List Total	Pop Hits	Pop Total	Fold Enrichment	Bonferroni	Benjamini	FDR
Downregulated genes											
GO Cellular Component	GO:0005886 plasma membrane	129	20,03	2,28E-07	460	2906	15855	1,53	7,33367E-05	7,33367E-05	0,000308455
Panther Molecular Function	MF00142 Lipase	11	1,70	3,39E-05	402	75	14744	5,38	0,005713312	0,005713312	0,041311999
GO Biological Process	GO:0006629 lipid metabolic process	48	7,45	7,21E-08	417	696	14219	2,35	0,000152055	0,000152055	0,000124685
GO Molecular Function	GO:0003779 actin binding	23	3,57	2,88E-05	441	288	15404	2,789525069	0,018164982	0,018164982	0,042842681
UCSC Transription factor binding sites	AP1	275	59,91	6,86E-06	449	9952	19536	1,202296636	0,001206322	0,000402269	0,008415558
Upregulated genes											
GO Biological Process	GO:0006333 chromatin assembly or disassembly	12	2,09	2,47E-05	310	109	14219	5,049659663	0,038606609	0,038606609	0,041332877

**Only statistical significant (FDR-p<0.05) enrichments are shown*

Supporting Table S5. HCC-deregulated genes reverted by the genetic deletion of ATX.

HCC$^{\Delta ATX}$: *AlbEnpp2*$^{-/-}$ mice 30/14w post DEN/CCl_4 treatment; HCC: control littermate mice post DEN/CCl_4 treatment; wt: control oil-treated mice.

		HCC$^{\Delta ATX}$ vs HCC		HCC vs wt	
Gene symbol	**Gene description**	**p**	**FC**	**p**	**FC**
Akr1c18	aldo-keto reductase family 1, member C18	0.0113	-26.47	0.0003	190.29
Slc7a11	solute carrier family 7 member 11	0.0005	-12.95	0.0000	29.96
2310034O05Rik	RIKEN cDNA 2310034O05 gene	0.0043	-10.61	0.0002	29.72
Scd2	stearoyl-Coenzyme A desaturase 2	0.0113	-8.95	0.0032	12.33
Tspan8	tetraspanin 8	0.0146	-8.90	0.0007	26.33
Gldn	gliomedin	0.0170	-8.75	0.0001	62.23
Cbr3	carbonyl reductase 3	0.0000	-8.68	0.0000	8.48
Klrb1b	killer cell lectin-like receptor subfamily B member 1B	0.0259	-8.50	0.0007	35.27
5330417C22Rik	RIKEN cDNA 5330417C22 gene	0.0311	-7.82	0.0012	28.15
H19	H19 fetal liver mRNA	0.0493	-7.49	0.0092	14.44
Igfbp1	insulin-like growth factor binding protein 1	0.0217	-7.47	0.0018	17.12
Wfdc15b	WAP four-disulfide core domain 15B	0.0244	-7.47	0.0008	26.08
Gpc3	glypican 3	0.0225	-7.47	0.0003	35.90
Ly6d	lymphocyte antigen 6 complex, locus D	0.0340	-7.42	0.0025	19.87
Afp	alpha fetoprotein	0.0386	-6.58	0.0007	31.85
Spink3	serine peptidase inhibitor; Kazal type 3	0.0379	-6.00	0.0009	23.72
Pnpla5	patatin-like phospholipase domain containing 5	0.0002	-5.88	0.0000	7.31
Cpe	carboxypeptidase E	0.0370	-5.68	0.0009	20.59
Alox5	arachidonate 5-lipoxygenase	0.0202	-5.32	0.0004	16.66
Gm10664	predicted gene 10664	0.0024	-4.85	0.0004	6.63
B4galt6	UDP-Gal:betaGlcNAc beta 1.4-galactosyltransferase	0.0167	-4.61	0.0008	9.69
Pls1	plastin 1 (I-isoform)	0.0008	-4.59	0.0000	10.92
Lcn2	lipocalin 2	0.0212	-4.49	0.0019	8.21
Ifi27l2b	Interferon alpha-inducible protein 27 like 2B	0.0186	-4.44	0.0023	7.19
Fabp5 (av3)*	fatty acid binding protein 5 epidermal	0.0260	-4.41	0.0247	4.05
Tlr1	toll-like receptor 1	0.0226	-4.40	0.0024	7.60
Itih5	inter-alpha (globulin) inhibitor H5	0.0219	-4.30	0.0013	8.72
Ngf	nerve growth factor	0.0143	-4.19	0.0029	5.73
Miox	myo-inositol oxygenase	0.0047	-3.97	0.0004	5.98
Nrg1	neuregulin 1	0.0430	-3.92	0.0061	6.52
Bex1	brain expressed gene 1	0.0367	-3.88	0.0091	5.35
Asns	asparagine synthetase	0.0314	-3.81	0.0027	6.91
Egr1	early growth response 1	0.0354	-3.55	0.0026	6.64
Cd63	CD63 antigen	0.0197	-3.54	0.0009	6.85
Tff3	trefoil factor 3	0.0070	-3.52	0.0001	8.41
Ifi44	interferon-induced protein 44	0.0365	-3.52	0.0302	3.42
S1pr3	sphingosine-1-phosphate receptor 3	0.0109	-3.52	0.0016	4.88
Cib3	calcium and integrin binding family member 3	0.0007	-3.43	0.0000	5.30
Gprc5b	G protein-coupled receptor, family C, group 5, member B	0.0007	-3.38	0.0000	6.00
Igkv5-43	immunoglobulin kappa chain variable 5-43	0.0397	-3.37	0.0242	3.56

Mfge8	milk fat globule-EGF factor 8 protein	0.0218	-3.35	0.0045	4.47
Rbp1	Retinol binding protein 1, cellular	0.0285	-3.34	0.0062	4.48
Tstd1	thiosulfate sulfurtransferase (rhodanese)-like domain c	0.0295	-3.30	0.0005	8.32
Igkj1	immunoglobulin kappa joining 1	0.0430	-3.23	0.0260	3.43
Pygb	brain glycogen phosphorylase	0.0249	-3.18	0.0093	3.69
Il1f9	interleukin 1 family, member 9	0.0007	-3.16	0.0002	3.46
Oas1g	2'-5' oligoadenylate synthetase 1G	0.0124	-3.15	0.0012	4.62
Slc39a4	solute carrier family 39 (zinc transporter), member 4	0.0092	-3.12	0.0023	3.74
Col4a3	collagen type IV, alpha 3	0.0019	-3.05	0.0001	4.51
Gm3893 (av3)*	predicted gene 3893	0.0320	3.01	0.0181	-3.12

*FC: Fold change of differential expression (>3 shown); p: p-value; *denotes an average (av) value of multiple probesets (x); HCC: DEN/CCl4-induced HCC in wt mice; ΔATX: DEN/CCl4-induced HCC in AlbEnpp2$^{-/-}$ mice; wt: oil treated littermate wt mice; known HCC markers.*

Materials and Methods

Experimental disease models

Carbon Tetrachloride (CCl4) intoxication: Mice were injected intraperitoneally once with CCl_4 (0.5 ml/Kg, 1:4 in corn oil) and then were sacrificed 24 h after the last injection. For chronic intoxication, mice were administrated CCl_4 (0.5 ml/Kg, 1:4 in corn oil) twice a week for 2, 4, 8, 12 consecutive weeks, then were sacrificed 24 h after the last injection. The control mice (littermate controls) receive for the same period the same volume of corn oil.

Thioacetamide (TAA) intoxication: Mice were administrated intraperitoneally TAA diluted in saline (300 mg/kg) 3 times/wk for 4, 8, 12 consecutive weeks, then were sacrificed 24 h after the last injection. The control mice received for the same period the same volume of saline.

Concanavalin A (ConA) model: ConA diluted in saline was administrated i.v. (15 mg/Kg). In control mice saline was administrated. The mice were sacrificed 24 h after the injection.

Lysophosphatidylcholine (LPC) in vivo: LPC (18:1) diluted in PBS/BSA was administrated i.v. (60 mg/Kg). In control mice PBS/BSA was administrated. The mice were sacrificed 3h, 6h, 12h and 24 h after the injection.

Diethylnitrosamine (DEN)/CCl4 model for HCC induction: Male mice were selected for these studies because male gender is a risk factor for human HCC. There were 4 groups for each genotype. At 2 weeks of age, mice in Groups 1 and 3 were injected i.p with sterile PBS (15 μl/g) vehicle. At the same age, mice in groups 2 and 4 were injected i.p with DEN (50 mg/kg) in sterile saline (15 μl/g). At 8-10 weeks of age (6-8 weeks after a single injection of DEN or vehicle as detailed above), mice in groups 1 and 2 were injected i.p biweekly with sterile corn oil (2 ml/kg), and mice in groups 3 and 4 were injected i.p biweekly with CCl_4 (0.5 ml/kg) diluted 1:4 in corn-oil vehicle for up to 12 additional weeks. Mice were sacrificed 30 weeks after the initial DEN injection.

Partial Hepatectomy (PH) 2/3 PH was performed essentially as previously described [PMID: 18600221]. The mice were anesthetized with 2% isoflurane. A midline abdominal skin and muscle incision (about 3 cm long) were made. After gently pulling down the median lobe with a saline-moistened cotton tip, the falciform ligament was cut. A 4-0 silk thread was placed on the base of the left lateral lobe (close to the liver hilum) using the micro dissecting forceps. With a cotton tip, the left lateral lobe were rotated to its original position, while holding the right end of the suture with the micro dissecting forceps, to make the suture go around the lobe. With the help of the microsurgery needle holder and the micro dissecting forceps, the suture was tied over the top of the left lateral lobe, placing the knot as close to the base of the lobe as possible. The thread for the second knot was placed between the stump and the median lobe. The median lobe was pull down over the suture and the knot was placed above the gall bladder, but no closer than 2 mm from the suprahepatic vena cava. When tying the second knot, the suture itself will section across the lobe. The tied median lobe was cut above the suture, leaving an ischemic stump above the knot and a small part of still perfused

median lobe below it. The peritoneum was closed with a 5-0 suture and the skin with 4-0 sutures.

Tissue and blood collection

At the end of treatment schedules, animals were sacrificed by decapitation and samples (blood/liver) were collected: Blood samples were obtained by cardiac puncture and drawn into eppendorf tubes containing 50mM EDTA. The plasma was immediately separated by centrifugation at 2000 g for 20 min at 4^0C, and aliquoted samples were transferred to polypropylene micro tubes and in siliconized tubes and stored at -80^0C. Liver was removed after perfusion with ice-cold sterile PBS, washed with ice cold saline to remove extraneous materials and was divided into 4 specimens. The first specimen (median lobes, left lateral lobe, quadrate lobe) was used for the histopathological examination. The liver was fixed in 4% buffered paraformaldehyde for 18–36 h and then paraffin embedded. The second specimen (half of the right lateral lobe) was stored at −70◦C used for the assessment of the hydroxyproline. The third specimen (half of the rest right lateral lobe) was blocked in OCT for cryosections. The fourth specimen (caudate lobe) was divided into 3 pieces (one for RNA, one for protein and one for lipid isolation) that were stored at -70^0C.

Liver histology and pathology

Liver specimens were preserved in 4% paraformaldehyde and dehydrated in a graded alcohol series. Specimens were then embedded in paraffin blocks, cut into 5 μm-thick sections, and placed on glass slides. Sections were then stained with hematoxylin and eosin (H&E) by a normal procedure and with Sirius red (0.1% Direct-Red-80 in saturated aqueous solution of picric acid at pH 2.0) for 1 h. Sirius red staining was used to grade the extent of fibrosis according to Ishak scoring system and H&E stained sections to assess the remaining histological parameters (necrosis, inflammation, steatosis, hydropic changes).

Hepatic fibrosis was graded according to Ishak scoring system: Grade 0: no fibrosis; grade 1: fibrous expansion of some portal areas with or without short fibrous septa, grade 2: fibrous expansion of most portal areas, with or without short fibrous septa, grade: 3: fibrous expansion of most portal areas with occasional portal to portal (P-P) bridging, grade 4: fibrous expansion of portal areas with marked bridging [portal to portal (P-P) as well as portal to central (P-C)], grade 5: marked bridging (P-P and/or P-C) with occasional nodules (incomplete cirrhosis), grade 6: cirrhosis, probable or definite. The cumulative histologic scores could have ranged from 0 (entirely normal) to 6 (severe disease with cirrhosis). Steatosis was scored by the percentage (%) of liver cells containing fat: 0 (<5%), 1 (5–33%), 2 (>33–66%) and 3 (>66%).

Hepatic disease activity for chronic hepatitis was graded by analysis of portal or lobular inflammation and necrosis according to Ishak modified Knodell Histology Activity Index (HAI) scoring system. This score does not include diffuse sinusoidal infiltration by inflammatory cells.

Modified HAI Grading: Necroinflammatory Scores

Piecemeal necrosis (A)	Score	Focal (spotty) Lytic Necrosis, and focal inflammation (B)	Score	Portal inflammation (C)	Score
Absent	0	Absent	0	Absent	0
Mild (focal, few portal areas)	1	One focus or less per 10x objective	1	Mild, some or all portal areas	1
Mild/moderate (focal, most portal areas)	2	Two to four foci per 10x objective	2	Moderate, some or all portal areas	2
Moderate (continuous around <50% of tracts or septa)	3	Five to ten foci per 10x objective	3	Moderate/marked, all portal areas	3
Severe (continuous around >50% of tracts or septa)	4	More than ten foci per 10x objective	4	Marked, all portal areas	4

Hepatic disease activity for acute hepatitis was graded as follows: *Necrosis*: Grade 0: Normal histology; Grade 1: Presence of degenerated hepatocytes with only rare foci of necrosis; Grade 2: Mild centrilobular necrosis around the central vein, occupying only a part of Rappaport's zone III; Grade 3: Established necrosis limited to zone III; Grade 4: Extensive, confluent centrilobular necrosis involving Rappaport's zone III and II. *Inflammation:* Lobular inflammation was quantified by assessing the number of inflammatory foci per microscopic field. Five fields were checked at 100× magnification as follows: 0 (absent), 1 (<2 foci), 2 (2–4 foci), and 3 (>4 foci).

Trichrome Stain

Liver was deparaffinized in xylene and rehydrate through 100% alcohol, 70% alcohol, 50 % alcohol and re-fixed in Bouin's solution for 1 hour at 56^0C to improve staining quality. After rinsing in running water for 5-10 minutes to remove the yellow color, liver tissue was stained in Weigert's iron hematoxylin working solution for 10 minutes. After, rinsing very well in running tap water until the water come clear (5-10 minutes) and washing in acidified water, the samples were stained in Biebrich scarlet-acid fuchsin solution for 5 minutes, washed in distilled water several times and were transferred to phosphomolybdic-phosphotungstic acid solution 1% for 5 minutes or until collagen is not red. Finally, samples were stained with aniline blue solution for 10 minutes, then transferred to phosphomolybdic-phosphotungstic acid solution 1% for 3 minutes and to 1% acetic acid solution for 2 minutes. The slides were mounted in GPX after quickly dehydration from ethanol to xylene.

Oil Red-O staining

Oil red O staining was done using freshly isolated liver tissue which was fixed in OCT and frozen at -80^{o}C. Frozen tissues were sectioned at 12 um. After equilibration of the tissue at RT for 10 min, liver sections were stained with Oil red O. ORO stock solution (0.6% in isopropyl alcohol) was mixed by magnetic stirring for 2 h at room temperature. ORO working solution was made fresh by dilution of 1.5 parts of ORO stock solution with one part of distilled water. After filtration it was applied to the tissue for 5 min. After washing with water, the slides were mounted with a water-soluble mounting medium. Lipid (Oil Red O) Staining Protocol in HepG2 following LPA treatment was performed with a protocol from Biovision. In detail, culture media from cells was aspirated and gently the cells washed 2 times with PBS. Formalin (10%) was added to each well and incubated for 30 min. After washing of cells 2 times with dH_2O, isopropanol (60%) was added and incubated for 5 min. Then the cells were incubated with Oil Red O working solution (the same used for the tissue) for 10-20 min under rotation. Excess staining was removed by washing 2-5 times with dH_2O until excess stain is no longer apparent. Some cells were mounted with mowiol on microscope slide and some other washed 3 times with 60% isopropanol. Oil Red O stain was extracted with 100% isopropanol for 5 min. with gentle rocking. Absorbance of the extracted isopropanol at 492 nm was measured in a spectrophotometer. The absorbance was proportional to Oil-Red O staining. 100% isopropanol was used as background control to subtract the background signal.

Periodic Acid Shiff Stain (PAS) for glycogen

5 µm sections of paraffin embedded liver were deparaffinized and hydrated to water. After oxidation in 0.5% periodic acid solution for 5 minutes and rinsing in distilled water, the slides were incubated with Schiff reagent for 15 minutes. Washing with lukewarm tap water for 5 minutes turn tissue from light pink to dark pink color. Counterstaining in Mayer's hematoxylin for 1 minute and mounting in GPX after quickly dehydration from ethanol to xylene.

X-gal staining

Freshly isolated mouse tissues were embedded in OCT and frozen in liquid nitrogen. Sections of 6 µm were prepared on a cryotome and fixed in 2 % formaldehyde/ 0.2 % glutaraldehyde for 10 minutes at 4°C, washed twice in cold PBS /2 mM $MgCl_2$ for 10 minutes and stained in X-gal staining solution (2 mg/ml X-gal (5-bromo-a-chloro-3-inodyl-β-D-galactopyranoside) in 0.1 M Na phosphate buffer pH 7.3, 0.01 % Na deoxycholate, 5 mM $K_3Fe(CN)_6$, 5.7 mM $K_4Fe(CN)_6$, 2 mM $MgCl_2$, 0.02 % NP-40) at 37°C in the dark overnight. The sections were rinsed twice in PBS /2 mM $MgCl_2$ for 10 minutes at room temperature, counterstained with eosin, and visualized under the microscope.

TUNEL was performed according to TUNEL kit supplied by promega according to manufacturer instructions.

ATX-In situ-hybridization

The hybridization was performed according to the protocol of QuantiGene view RNA ISH Tissue Assay for formalin embedded tissue of Affymetrix. Riboprobes for ATX were purchased by Affymetrix.

Liver Hydroxyproline measurement

Snap-frozen liver tissue (50–60 mg each) was hydrolyzed at 110°C for 16 h in 1 mL 6N HCl. The hydrolysate was evaporated to dryness and reconstituted in 100 µl of acetate/citrate buffer (57 g sodium acetate · $3H_2O$, 37.5 g trisodium citrate · $2H_2O$, 5.5 g citric acid · H_2O, 385 mL isopropanol, and dissolved in H_2O to a final volume of 1 L), filtered and 25-µL aliquots were removed to a 96-well plate and oxidized in each well with a solution containing 130 µL of 0.056 M Chloramine T in acetate/citrate buffer and incubated at room temperature for 20 min. Thereafter 130 µL of Ehrlich's solution 1 M was added. The Ehrlich's solution was prepared by dissolving 1.5 g of p-dimethylamino-benzaldehyde in 2.5 mL of 60% $HClO_4$ and then mixed with 7.5 mL of isopropanol. The final mixture was incubated at 60°C for 1h and then at room temperature for 10 min, and the absorbance was determined at 560 nm. Standard solutions containing 0-500 µg/mL of authentic 4-hydroxy-L-proline (Sigma) were treated likewise. The standard curve was linear in this range (r = 0.98). The value of the liver hydroxyproline level was expressed as µg /mg wet tissue and transformed to µg collagen/mg tissue using the following equation: Collagen content (µg/mg tissue)= Hydroxyproline (µg/mg tissue)/(dilution factor*7.5).

Immunohistochemistry

Paraffin embedded tissue and OCT embedded tissues were cut at 5 µm. The paraffin-embedded tissue slices were baked at 60ºC for about 60 minutes to melt the paraffin, de-waxed using xylene and rehydrated with an alcohol gradient. Microwave antigen retrieval was performed at 95°C for 10-15 minutes using a citrate buffer (pH 6.0) or Tris-EDTA (pH8 and pH9) depending on the 1ry ab used. They were then incubated with a hydrogen peroxide (3%)-water solution for 15 minutes to inactivate endogenous peroxidase. A blocking solution containing 1% BSA/2% normal serum of the same species as the secondary antibody was incubated with the sample for 45-60 min in a humidifying chamber to block non-specific antibody binding. Primary antibodies diluted in 1% BSA in PBST were incubated with the tissue sections overnight at 2-8 °C. Secondary abs diluted in 1% BSA in PBST were applied for 1 hour at room temperature. HRP-conjugated abs (1:1000 dilution), biotinylated secondary antibodies (1:1000) or Alexa-conjugated abs (1:500) were used. For biotinylated secondary abs, tissue was incubated further with-HRP conjugate for 30 minutes. DAB chromogenic solution was applied for 1-5 min. The reaction was stopped in water. Hematoxylin counterstain and mounting in GPX. For fluorescent staining nuclei was stained with DAPI (1:2000 dilution in PBS) for 5 min. The scoring of frequency and intesity of the staining was performed with the Image-J (scoring of 7 independent fields in at least 3 mice).

Abs and antigen retrievals used in IHC

	1ry Ab	2ry ab	Antigen Retrieval
anti-ATX (Cayman)	2 μg/ml	goat-anti-rabbit HRP (Southern-Biotech)	Sodium Citrate 10 mM pH 6, 0.05% Tween-20
anti-ATX (7A5)	4 μg/ml	goat-anti-mouse A555 (Invitrogen)	50 mM TrisPH8, 1 mM EDTA, 0.05% Tween-20
Albumin	1:250	donkey-anti-goat A555 (Invitrogen)	Sodium Citrate 10 mM pH 6, 0.05% Tween-20
aSMA (Thermo Fisher Scientific)	0.4 μg/ml	goat-anti-mouse A555 (Invitrogen)	Sodium Citrate 10 mM pH 6, 0.05% Tween-20
PCNA (Abcam) permeabalization for 10 min in 0.1% Tritox-X	0.1 μg/ml	goat-anti-mouse HRP (Southern-Biotech)	Sodium Citrate 10 mM pH 6, 0.05% Tween-20
CD68 (Abcam) permeabalization for 10 min in 0.1% Tritox-X	1:50	Biotinylated anti-rat (Vector)	Cryosection
F4/80 (Serotec)	20 μg/ml	Biotinylated anti-rat (Vector)	Sodium Citrate 10 mM pH 6, 0.05% Tween-20
CD3 (Abcam)	1:100	Biotinylated anti-rabbit (Vector)	Sodium Citrate 10 mM pH 6, 0.05% Tween-20
B220 (BD Bioscience)	0.25 μg/ml	Biotinylated anti-rat (Vector)	Sodium Citrate 10 mM pH 6, 0.05% Tween-20
Gr-1 (Abcam)	2 μg/ml	Biotinylated anti-rat (Vector)	Sodium Citrate 10 mM pH 6, 0.05% Tween-20
CD34 (Abcam)	1:250	goat-anti-rabbit HRP (Southern-Biotech)	Tris-EDTA pH 9

Retinoic acid measurement

Retinoic acids (13-cis and all-trans RA) were measured in plasma with an HPLC-DAD method. Briefly, 50 μl plasma were deproteinized with 150 μl of acetonitrile by vortex for 1 min and centrifugation at 3000 rpm at 4^{o}C. The supernatant was filtered and injected a Betabasic C18 (250x4.6 mm, 5 μm particle size) column, protected by a 10 x 4 mm guard column filled with the same material as the column (Thermo Scientific) of the HPLC system (Agilent Technologies , Hewlett Packard 1100, USA). The mobile phase was a mixture of acetonitrile, methanol, tetrahydrofuran and sodium acetate 100 mM adjusted to pH 5.4 with acetic acid, (43:35:7:15 by volume). The analysis was performed under isocratic conditions and in a flow rate of 1 mL/min. The detection wavelength was set at 350 nm. All data were automatically stored on disk. The HPLC system was controlled by the software installed on a personal computer system. For determination of elution times, each standard retinoid (Sigma Aldrich) was injected alone and the corresponding retention time was recorded.

Isolation of primary liver cells

Liver cells were isolated with two-step collagenase perfusion. After *in-situ* perfusion with HBSS and collagenase (1 mg/ml in HBSS with Ca^{2+}) the liver was collected with a curved

spatula and transferred into a plate where the disruption of the tissue is preceded with a scalpel. 5 ml of warm collagenase was added and the liver was cut into very small pieces very quickly and incubated for further 30 min in 37^{O}C in Eyrleimener flask. Minced tissue was collected and cells were filtered through 70 μm cell strainer. After washing the strainer up to 30 ml final with culture media, the cells with media were split in 2x15 ml falcon tubes.

Hepatocytes isolation. Cells were centrifuged at (50g) for 5min at 4^{o}C. The supernatant (S1) was kept on ice for subsequent nonparechymal cell (NPC) isolation. The pellet was resuspended in 7 ml DMEM and was passed gently on the top of 7 ml 90% percoll to recover viable cells. After centrifugation at 50 g for 5 min at room temperature, the pellet of viable cells was washed in culture media and resuspended in culture media for plating.

NPC Isolation. S1 containing NPC, red blood cells, hepatocytes, and debris was centrifuged at 580 g for 10 minutes at 4°C to enrich the NPC. The pelleted cells were gently resuspended in 20 mL of Dulbecco's PBS with Ca^{2+} containing 0.3% bovine serum albumin (BSA) with pronase-E and incubated at 37^{o}C for 30 min to destroy remaining hepatocytes. After centrifugation at 500 g for 10 minutes at 4°C the pelleted cells were gently resuspended in 20 mL of Dulbecco's PBS without Ca^{2+} or Mg^{2+} containing 0.3% BSA. The cell suspension was mixed with 16 mL of 27.6% (wt/vol) of Nycodenz, giving a final concentration of 13% (wt/vol), and centrifuged at 900 g for 30 minutes at 4°C. HSC, LEC, and Kupffer cells (KC) were found above the Nycodenz cushion, whereas the lymphocytes, red blood cells, and the debris were pelleted. The NPCs were then removed, diluted up to a volume of 50 mL in PBS-BSA, shaken at 150 rpm for 30 minutes at 4°C in an environmental incubator shaker, and then centrifuged at 580 g for 10 minutes at 4°C. To separate the HSC from the LEC and the KC, the cell pellet was gently resuspended in 6 mL of PBS-BSA solution and mixed with 6.6 mL of 100% Percoll (9 parts Percoll diluted with 1 part 10-fold-concentrated PBS). 2 ml of this cell suspension was under-layered a two-step Percoll gradient (4 ml of 50% Percoll, 4 ml of 35% Percoll, and 1 ml of PBS-BSA; 10-mL centrifugation tubes were used) and centrifuged at 900 g for 30 minutes at 4°C. 3 different cell bands were obtained: one at the top of the Percoll gradient enriched in HSC (fraction 1), one at the interface between the two Percoll cushions mainly enriched in LEC (fraction 2), and one near the bottom of the centrifugation tube enriched in KC (fraction 3). The fraction 3 as well as the combined fraction 1 and 2 washed to remove the Percoll solution and centrifuged at 300 g for 15 min.

HSC isolation. After *in-situ* perfusion with EGTA solution pH 7.4 (NaCl 8 g/lt, KCl 0.4 g/lt, $NaH_2PO_4 \cdot H_2O$ 0.08 gr/lt, Na_2HPO4 0.12 g/lt, HEPES 2.3 g/lt, $NaHCO_3$ 0.35 g/lt, EGTA 0.19 g/lt, Glucose 0.9 g/lt), pronase (0.4 mg/ml) and collagenase (0.09 U/ml) in digestion buffer pH 7.4 (NaCl 8 g/lt, KCl 0.4 g/lt, $NaH_2PO4 \cdot H_2O$ 0.08 gr/lt, Na_2HPO_4 0.12 g/lt, HEPES 2.3 g/lt, $NaHCO_3$ 0.35 g/lt, $CaCl_2 \cdot 2H_2O$ 0.56 g/lt) the liver was collected with a curved spatula and transferred into a plate where the disruption of the tissue is preceded with a scalpel. 5 ml of warm collagenase (0.09 U/ml) /pronase (0.4 mg/ml) with 1% DNAase in digestion buffer was added and the liver was cut into very small pieces very quickly and incubated for further 25 min in 37^{O}C in Eyrleimener flask. Minced tissue was collected and cells were filtered through 70 μm cell strainer in a 50 ml falcon. The cells were centrifuged at 580g for 10min at 4^{o}C. The supernatant was aspirated until 10 ml remains in the tube, and

then 120 µl of DNase I was added with GBSS/B pH 7.4 (KCl 0.37 g/lt, $MgCl_2 \cdot 6H_2O$ 0.21 g/lt, $MgSO4 \cdot 7H_2O$ 0.07 g/lt, Na_2HPO_4 0.06 g/lt, KH_2PO_4 0.03 g/lt, glucose 0.9 g/lt, $NaHCO_3$ 0.28 g/lt, $CaCl_2 \cdot 2H_2O$ 0.225 g/lt) until 50 ml. The cells were centrifuged at 580g for 10 min at 4 °C. After aspiration of the supernatant until 10 ml remains in the tube, 120 µl of DNase I was added and the pellet was resuspended with a 10-ml pipette. 32 ml of GBSS/B was added following by 16 ml of 0.2 g/ml Nycodenz in GBSS/A (GBSS/B with 8 g/lt NaCl). 12 ml of cell-Nycodenz suspension was added into each of the four 15-ml Falcon tubes (previously moistened), and was overlayed with 1.5 ml of GBSS/B using a 3-ml syringe with a 26-gauge needle attached. The suspension was centrifuged at 1,380g for 17 min (4°C) without brake. At the end of centrifugation, the HSCs were visible as a thin white layer in the interface between the cell-Nycodenz solution and the overlay with GBSS/B. With a 5-ml pipette, the cells were collected and were transferred into a new 50-ml Falcon tube filled with GBSS/B, were gently mixed and centrifuged at 580g for 10 min at 4°C. The pellet was resuspended in DMEM with 10% FBS and used immediately for cell culture. Purity of HSC (80%) was confirmed by FACS analysis based on Vitamin A auto fluorescence.

Cell culture

Hepatocytes (Heps) were plated on collagen I-coated plastic dishes (1-2x10^6 live cells/ml) at 6 well plates and cultured in DMEM medium with the addition of 10% FBS, 1% penicillin/streptomycin (P/S), 1% Insulin Transferrin Selenium, 250 ng/ml Fungisone, 2 mM Glutamine for 6 hours and after removal of the culture media were cultured for further 1 day. Purity was confirmed by FACS analysis before plating and was about 90%.

Liver Sinusoidal Endothelial cells (LSEC) with Hepatic Stellate Cells (HSC) were plated on collagen I-coated plastic dishes (1-2x10^6 live cells/ml) at 6 well plates and cultured in DMEM medium with the addition of 20% FBS, 1% P/S, 250 ng/ml Fungisone, 2 mM Glutamine for 1 day.

HSC were cultured for 3 days in DMEM medium with the addition of 10% FBS, 1% P/S, 250 ng/ml Fungisone, 2 mM Glutamine.

Kupffer cells were cultured in plastic dishes (1-2x10^6 live cells/ml) at 6 well plates, containing RPMI medium with 10% FBS and 1% P/S for 1 day after selective plating for 15 min in plastic dish.

Huh7.5 and Hep2G cells were maintained in Dulbecco's modified Eagle medium (high glucose for Huh7.5/ low glucose for HepG2 cells) supplemented with 2 mM glutamine, 10% (v/v) heat-inactivated fetal calf serum and 100U/ml penicillin/streptomycin and non-essential amino acids.

***In vitro* cell treatments**

After 1 day culture all the cells was serum-starved for 24 hours with 0.1% BSA and were treated for 24 hours with LPS (100 ng/ml), LPC 18:1 and/or LPC 16:0 (5-50 µM), recombinant mouse TNF (10 ng/ml), all-trans RA (1 µM), LPA 18:1 (10 µM). Cell lysate in trizol and supernatant were kept at -80^{o}C for analysis. Viral infections of permissive Huh7.5 cells with the JFH-1 infectious clone (HCV strain genotype 2a) were done at multiplicity of

infection=1, essentially by incubating viral particles with cells for 4h, removing the inoculum and adding fresh medium 4. In vitro transcription of the JFH1 (wt) and the corresponding replication-incompetent mutant (JFH1/GND) was carried out using the T7 RiboMAX™ Express Large Scale RNA Production System (Promega). Transfection of the RNA transcripts was performed in HepG2 cells. Briefly, 100,000 cells/well were seeded in 48-well plates 24h prior to the experiment. Cells were electrotroporated with 10μg RNA and equal amounts of carrier t-RNA in Cytomix buffer (12mM KCl, 0.15mM $CaCl_2$, 10mM K_2HPO_4/KH_2PO_4 pH 7.6, 25mM Hepes, 2mM EGTA, 5mM $MgCl_2$, 2mM ATP and 5mM reduced glutathione). Following transfection, cells were harvested at the appropriate time points and subjected to luciferase and β-galactosidase activity measurements with commercially available kits (Promega). Luciferase activity was normalised to β-galactosidase activity in order to yield relative luciferase activity (RLA). Each transfection was carried out at least 3 times in triplicate.

Phallodoin staining

Cells fixed at fresh 4% Paraformaldehyde for 15 min at 2-8 °C and permeabilized with 0.1% Tritox-X in PBS for 10 min. Then, tissues were incubated with Phalladoin-Alexa 555 (1:500 dilution in PBS) for 1 hour. Nuclei were stained with DAPI (1:2000 dilution in PBS) for 5 min.

MTT Assay

Cells were grown on 96 well plates. After the treatment, supernatant was aspirated and the cells were washed 3 times with DMEM phenol free. MTT (0.5 mg/ml) diluted in DMEM Phenol free was added (150 ul) and was incubated for 3 hours at 37^{o}C. 75 ul acidic propanol (with 0.04 N HCL) was added and after 30 min incubation at RT under rotation, the absorbance of solubilized crystals were measured at 570 nm. After subtraction of background at 630-690 nm, the resulting absorbance was expresses as % of the absorbance of untreated cells.

Immunocytochemistry

Cells fixed at fresh 4% Paraformaldehyde for 15 min at 2-8 °C. Blocking of non-specific binding performed with 5% BSA for 60 min in a humidifying chamber. Primary antibodies (Cayman anti-ATX, 2 μg/ml, aSMA 1:100) diluted in 1% BSA were incubated with the tissue sections overnight at 2-8 °C. Alexa secondary abs diluted 1:1000 in 1% BSA in PBST were applied for 1 hr at room temperature. Nuclei were stained with DAPI (1:2000 dilution in PBS) for 5 min.

Production of a-ATX Monoclonal Antibodies

Human Enpp2 cDNA was purchased from OpenBiosystems and was subcloned into a mammalian expression vector with an 8His tag at the C-terminus to generate pLEXm-hEnpp2-8H. Purified plasmid DNA was transfected into 293T cells and the secreted hEnpp2-8H protein was purified form the conditioned medium by the combination of conventional and affinity chromatograph methods. Purified protein (0.5 and 2ug) was examined on a SDS gel and showed more than 95% homogeneity. The specificity of the protein (0.25 and 1ug)

was confirmed by the Western blot using the antibody against His tag. Protein concentration was determined using the Protein Assay (BioRad) and the endotoxin level was measured <10EU/mg using the QCL-1000 kit (Lonza).

1 mg of hEnpp2-8H protein was sent to Absea Biotechnology Ltd for the production of anti-ATX monoclonal antibodies. Following fusion, the supernatants from 17 hybridomas were tested against the antigenic recombinant hATX with ELISA; 11 selected clones were then grown in serum-free medium (Gibco, Paisley, Scotland, UK) and the antibodies from their supernatants were purified by affinity chromatography with Protein A (ProSep®-vA High Capacity chromatography, Millipore). All 11 clones were tested in direct and indirect ELISAs, western blots and immunohistochemistry. Selected clones, 7A5 for fluorescence immunohistochemistry, and 13H8 for western blots, were all determined as IgG1 isotypes.

Hyaluronic acid (HA) measurement: The HA was measured with an Elisa kit obtained from My Bio source.

HPLC-ESI/MS/MS lipid analysis was performed using HPLC-ESI/MS/MS using RSLCnano system (Ultimate 3000) coupled in-line with an LTQ Orbitrap XL mass spectrometer (Thermo Scientific, Waltham, MA, USA). Lipid extraction was performed on ice according to the Folch method with minor modification. Plasma samples (50 ul), mixed with 450 ul PBS/liver tissue (20-50mg) homogenized at 0.5 ml PBS/ cells harvested in 500 µl PBS were spiked with the internal standard mix (17:1 LPA/LPC/LPI/LPE/LPG/LPS, 17:1 S1P, 19:0 PC, PE, PS, PG, 17:0/17:0/17:0 TAG, 17:/17:0 DAG). Samples were extracted under neutral conditions with 2 ml of ice-cold methanol/chloroform (2/1, v/v) followed by 1 ml of ice-cold chloroform. 0.5 ml water was added to separate the 2 phases. Each extraction step was followed by a 60 s vortex and a 10 min centrifugation step in a bench-top clinical centrifuge in a cold room at 4°C at 3,000 rpm. The lower chloroform organic phases from both neutral extraction steps were pooled and kept for TAG, DAG, MAG, CE, SM, SPC, PC, LPC, LPE, PE,measurement. The remained aqueous phase was chilled on ice for 10 min and acidified with HCl to pH 2-3. 2 ml of chloroform/methanol (2/1, v/v) was added as above. The lower organic phases were pooled, neutralized to pH 6–7 (checked with pH paper as above) on ice and kept for LPA, S1p LPI, LPS, LPG, PS, PI, PG, PA measurements. The kept neutral lower organic phase of neutral extraction and the neutralized acidified lower organic phase were evaporated to dryness. The resulting residues were resuspended in isopropanol and after brief vortex mixing the solution was transferred to the auto sampler vial. Recovery of most lipid species was between 60% and 95%. The Relative Standard Deviation (RSD) was less than 7% from the plasma fortified with 4 different concentrations of LPA, LPC, PC, standards. Analysis was performed using a Phenomenex (Phenomenex, Torrance, CA, USA) Luna Silica column (2–250 mm, 5 µm particle size) using a binary gradient program consisting of isopropanol:hexane:100 mM NH_4CO_2H(aq) 58:40:2 (mobile phase A) and isopropanol:hexane:100 mM NH_4CO_2H(aq) 50:40:10 (mobile phase B). The mobile phase was delivered at a flow rate of 0.3 ml/min and the total run time was 50 min/sample. The analysis was performed with electrospray ionization in SIM (Single Ion Monitoring) mode for LPA species and in data dependent MS/MS for all other lipids. The resolution was 100 K providing high accuracy for lipids measurements. The analysis of different lipid classes was

based on the retention time of different commercial standards (avanti polar lipids), on their precursor ion mass and on their isotope distribution. The precursor ion mass was used for the ion intensity record while lipid identity was confirmed by precursor ion fragmentation using collision induced dissociation (CID). All the ion intensities of the lipids were normalized to the ion intensity of the corresponding internal standard (AU). Standard curves was performed for LPA, LPC, species with standard lipids obtained by Avanti. The peak area ratios (lipid/internal standard) versus the molar ratios (lipid/internal standard) were plotted and fitted to a linear regression. Positive ion mode FT MS analysis with scan ranges m/z 100-1500 m/z , monitors PC, LPC, LPE, SM, Cer, DAG, PE, CE, MAG and TAG species while negative ion mode FT MS analysis used for LPS, LPI, PA, PS, PI, PG species). All FT MS spectra were acquired in profile mode. For the liver lipids, the normalized to internal lipids were normalized also for the weight of the liver sample. For HepG2 cells, the TAG were normalized to cells total protein measured with Bradford.

Lipid names and abbreviations (Abb)

Abb	Name	Abb	Name
TAG	Triacyloglycerol	Cer	Ceramide
DAG	Diacyloglycrerol	S1p	Sphingosine 1 Phosphate
MAG	Monoacyloglycerol	CE	Cholesterol Esters
SM	Sphingomyelin	SPC	Sphingophosphorylocholine
PI	Phosphatidyloinositole	LPI	Lysophosphatidyloinositole
PC	Phosphatidylocholine	LPC	Lysophosphatidylocholine
PE	Phosphatidyloethanolamine	LPE	Lysophosphatidyloethanolamine
PS	Phosphatidyloserine	LPS	Lysophosphatidyloserine
PA	Phospatidic acid	LPA	Lysophosphatidic acid

ATX ELISA

Samples and standards were diluted in coating buffer (12 mM $NaCO_3$ and 28 mM $NaHCO_3$, pH 9.6) and incubated overnight at 4^{o}C in 96-well plate (NUNC). Serum samples were diluted 1:50 after titration. Recombinant ATX (C187-EN, R&D Systems) at concentrations (120-3.75) ng/ml was used to construct a linear standard curve. After blocking for 1.5 h with 2% BSA in PBS-T, samples were incubated with a-ATX goat anti-mouse antibody 1:500 for 2 hour. The α-ATX antibody was detected with horse anti-goat HRP conjugated antibody (PI-9500, Vector, UK) and developed with TMB (3,3',5,5'-tetramethylbenzidine, Sigma). The reaction was stopped with 2M H_2SO_4 and readings were obtained using a spectrophotometer at 450 nm.

ATX activity assay

ATX/LysoPLD activity was measured using the TOOS activity assay. ATX catalyzes the cleavage of lysophosphatidylcholine to lysophosphatidic acid and choline. The released choline is oxidised by choline oxidase to produce betaine and hydrogen peroxide. The latter is used as the oxidizing agent. In the presence of horseradish peroxidase, H_2O_2 reacts with TOOS (N-ethyl-N-(2-hydroxy-3-sulfopropyl)-3-methylaniline) and 4-AAP (aminoantipyrene) to form a pink quinoneimine dye which absorbs at 555 nm. 1 x LysoPLD buffer (100 mM Tris-HCl pH 9.0, 500 mM NaCl, 5 mM $MgCl_2$, 5 mM $CaCl_2$, 60 µM $CoCl_2$, 1 mM LPC) was incubated at 37°C for 30 minutes. Plasma samples (100 fold diluted) were incubated with 1 x LysoPLD buffer at 37°C for 4 hours at a final volume of 100 µl in a 96-well plate. At the end of the incubation, a colour mix (0.5 mM 4-AAP, 7.95 U/ml HRP, 0.3 mM TOOS, 2 U/ml choline oxidase in 5 mM $MgCl_2$/ 50 mM Tris-HCl pH 8.0) was prepared and 100 µl were added to each well. Absorbance (A) was measured at 555 nm every 5 minutes for 20 minutes. For each sample, the absorbance was plotted against time and the slope (dA/min) was calculated for the linear (steady-state) portion of each reaction. ATX activity was calculated according to the following equation: Activity (U/ ml) = (µmol/ min/ ml) = [dA/ min (sample) - dA/ min (blank)] * Vt/ (e* Vs* 0.5) where Vt: total volume of reaction (ml), Vs: volume of sample (ml), e: milimolar extinction coefficient of quinoneimine dye under the assay conditions (e = 32,8 µmol/ cm^2) and 0.5: the moles of quinoneimine dye produced by 1 mol of H_2O_2.

Western Blot

Homogenized liver tissue in RIPA buffer, was diluted in Laemmli buffer, electrophorised on 8% SDS-polyacrylamide gels (30-60 ugr of protein/lane) and transferred to Protran nitrocellulose membranes (Whatman plc) using the Trans-Blot SD Semi-Dry Transfer system (Bio-Rad Laboratories). Primary ab incubation (mouse monoclonal anti-ATX 13H8, mouse monoclonal a-SMA, rat tubulin) was performed overnight in 5% (w/v) non-fat milk in TBS-Tween 0.05% (TBST) at 4°C. The membranes were then washed three times with TBST and incubated with HRP-conjugated secondary Abs (a-mouse Fab2, r a-rat respectively; 1:2000) for one hour at room temperature. Membranes were washed three times with TBST and antibody-antigen complexes were revealed using ECL chemiluminescent reagent (Pierce/ Thermo Scientific).

RNA Extraction and Real-time RT-PCR Analysis

RNA was extracted from the liver using the Tri Reagent (TR-118) obtained from Invitrogen and treated with DNAse (RQ1 RNAse-free DNAse) prior to RT-PCR according to manufacturer's instructions. Reverse transcription was performed for cDNA synthesis using the MMLV reverse transcriptase obtained from promega. cDNA synthesis was performed using 4 µg of total RNA per sample with OligodT. Real-time PCR was performed on a BioRad CFX96 Touch™ Real-Time PCR Detection System (Bio-Rad Laboratories). Values were normalized to the expression of b-2 microglobulin (*b2m*) and/or hypoxanthine-guanine

phosphoribosyltransferase / *Hprt*. Total relative quantitation was calculated using the delta–delta cycle threshold (ΔΔCt) method or Standard curve method

Primer sequences (Forward:F; Reverse:R)

Gene	primer sequence (5'-3')	Gene	primer sequence (5'-3')
Acta2	F: CTGCTCCAGCTATGTGTGA	Lpar6	F: GATCACTCTCTGCATCGCTGTTTC
	R: TTACAGAGCCCAGAGCCATT		R: CCCTGAACTTCAGAGAACCTGGAG
B2m	F: TTCTGGTGCTTGTCTCACTGA	Lpcat3	F: GGCTCTGTTTTACCGGCATTA
	R: CAGTATGTTCGGCTTCCCATTC		R: GCAAGGAGTGGTAGAACTGGTG
Bax	F: TGAAGACAGGGGCCTTTTTG	NS3-2a	F: CTGCCACCCTGGGGTTTGGG
	R: AATTCGCCGGAGACACTCG		R: GCAGCCCCCATCGGCGAGAA
Bcl2	F:ACGTGGACCTCATGGAGTG	Pla2g12a	F: GCAACGGCATCCACAAGATAG
	R: TGTGTATAGCAATCCCAGGCA		R: CATAGCGTGGAACAGGCTTC
Col3a1	F: GCCCACAGCCTTCTACAC	Pla2g15	F: CAGCAAGAGGAATGTGGGTTC
	R: CCAGGGTCACCATTTCTC		R: CCGCCAATCATAGGGAGCAC
Cxcr4	F: AGCATGACG GACAAGTA	Pla2g16	F: GGACCCAAGCAAAGGCATCC
	R: GATGATATGGACAGCCTTACA C		R: CCAGCTCCTGCGATTTCACT
Cxcr7	F: AGCCTGGCAACTACTCTGACA	Pla2g1b	F: CACCCCAGTGGACGACTTAG
	R: GAAGCACGTTCTTGTTAGGCA		R: GCATTTGTTGTTTTTGGCGCT
Cyclin D1	F: CCAGGCCCAGCAGAAGGTCG	Pla2g6	F: GCAAGCTGATTACCAGGAAGG
	R: TCCCCAAGGGGGACGTCGTC		R: GAGAGAAGAGGGGGTGAGTTG
Cyp2s1	F:TCTCTGACGCTATTCAGGACC	Pla2g7	F: CTTTTCACTGGCAAGACACATCT
	R: CTTACTTAGCCGCAAAAGCCC		R: CGACGGGGTACGATCCATTTC
Enpp2	Taq Man Primers	Ppap2a	F: TGTACTGCATGCTGTTTGTCGCAC
			R: TGACGTCACTCCAGTGGTGTTTGT
ENPP2	Taq Man Primers	Ppap2b	F: ATAAACGATGCTGTGCTCTGTGCG
			R: TTTGCTGTCTTCTCCTCTGCACCT

Hgf	F: ATGTGGGGGACCAAACTTCTG	Ppap2c	F: TCCTTTGGCATGTATTGCATGT
	R:GGATGGCGACATGAAGCAG		R: AAGGCCACCAAGAAGAACTGA
Hprt	F: GGCCAGACTTTGTTGGATTT	Scd2	F: TCTTGGTTTCCATGGGAGCTG
	R: CAGATTCAACTTGCGCTCAT		R: AAGACCCCACACTCAGCCG
Il-1b	F: GCAACTGTTCCTGAACTCAACT	hSCD1	F: GCTACACTTGGGAGCCCTGT
	R: ATCTTTTGGGGTCCGTCAACT		R: ACATCATTCTGGAATGCCATTGTGT
Il-6	F: TAGTCCTTCCTACCCCAATTTCC	S1pr1	F:GGATCGCGCGGTGTAGAC
	R: TTGGTCCTTAGCCACTCCTTC		R:TTCTCCAGGCAAACGCTAGA
Lpar1	F: GAGGAATCGGGACACCATGAT	S1pr2	F: GCCAACAGTCTCCAAAACCA
	R: TGAAGGTGGCGCTCATCT		R: GAGTATAAGCCGCCATGGT
Lpar2	F: GACCACACTCAGCCTAGTCAAGAC	S1pr3	F:CTGAGACACGGCAGCATG
	R: CAGCATCTCGGCAGGAAT		R:TTCAACAGTCCACGAGAGGG
Lpar3	F: GCTCCCATGAAGCTAATGAAGACA	Tgfb	F: CTCCCGTGGCTTCTAGTG C
	R: TACGAGTAGATGATGGGG		R: GCCTTAGTTTGGACAGGATCTG
Lpar4	F: AGTGCCTCCCTGTTTGTCTTC	Tnf	F: CACGCTCTTCTGTCTACTGA
	R: GCCAGTGGCGATTAAAGTTGTAA		R: ATCTGAGTGTGAGGGTCTGG
Lpar5	F: ACCCTGGAGGTGAAAGTC		
	R: GACCACCATATGCAAACG		

Microarray hybridization and data analysis

300ng of total RNA (isolated with Trizol, purified with a single passage through RNeasy columns and digested with DNase on the column) were used to generate biotinylated complementary RNA (cRNA) for each treatment group using the "GeneChip® WT PLUS Reagent Kit protocol for Whole Transcript (WT) Expression Array, Rev3" and according to the manufacturer's instructions. In short, isolated total RNA was checked for integrity using the RNA 6000 Nano LabChip kit on the Agilent Bioanalyzer 2100 (Agilent Technologies, Inc., Palo Alto, CA) and concentration using the ND-1000Nanodrop (Thermo Fisher Scientific, Wilmington, Delaware USA). Poly-A RNA control added to the RNA test samples as exogenous positive control and the RNA was reversed transcribed to double stranded cDNA and biotinylated cRNA was synthesized and purified according to the protocol. A 2nd cycle of cDNA synthesis followed along with a second purification step. 6µg of the single-stranded DNA was fragmented, labeled with the appropriate labeling reagent and hybridized to GeneChip® MOGene 2.0 ST arrays. Hybridization took place for 16hrs in an Affymetrix GeneChip® Hybridization Oven 640. Affymetrix GeneChip® Fluidics Station 450 was then used to wash and stain the arrays with streptavidin-phycoerythrin according to the standard

antibody amplification protocol for eukaryotic targets. Arrays were on Affymetrix GeneChip® Scanner 3000 at 570nm. The Affymetrix eukaryotic hybridization control and Poly-A RNA control were used to ensure efficiency of hybridization and cRNA amplification. Images and data were acquired and analyzed using the Affymetrix® GeneChip® Command Console® Software (AGCC), where initial quality check of the experiment was performed. Command Console® Software (AGCC) was also used to perform RMA normalization and statistical analysis. Gene enrichments with their corresponding functions were analyzed by the online analysis engine "Database for Annotation, Visualization and Integrated Discovery" (DAVID) 6.7. The MIAME-compliant data set is publicly available (#E-MTAB-4648) at ArrayExpress.

Data minining of publically available microarray datasets

Raw datasets of patient samples were reanalyzed using the statistical environment R 2.14.1 (Biobase 2.15.3, GEOquery 2.23.2, limma 3.10.1). Raw data of patient and matching control were normalized using the RMA algorithm and Fold Change expression ratios were generated. Statistical significance was established by applying correction for multiple comparisons using Benjamini & Hockberg multiple test correction (FDR).